Defense Threat Reduction Agency
8725 John J. Kingman Road, MS
6201 Fort Belvoir, VA 22060-6201

DTRA-TR-16-68

TECHNICAL REPORT

Neutralization of Aerosolized Bio-agents by Filled Nanocomposite Materials through Thermal and Chemical Inactivation Mechanisms

June 2016

HDTRA1-11-1-0017

Sergey Grinshpun et al.

Prepared by:
University of Cincinnati
Cincinnati, OH 45267

DESTRUCTION NOTICE:

Destroy this report when it is no longer needed.
Do not return to sender.

PLEASE NOTIFY THE DEFENSE THREAT REDUCTION AGENCY, ATTN: DTRIAC/ J9STT, 8725 JOHN J. KINGMAN ROAD, MS-6201, FT BELVOIR, VA 22060-6201, IF YOUR ADDRESS IS INCORRECT, IF YOU WISH IT DELETED FROM THE DISTRIBUTION LIST, OR IF THE ADDRESSEE IS NO LONGER EMPLOYED BY YOUR ORGANIZATION.

REPORT DOCUMENTATION PAGE

Form Approved
OMB No. 0704-0188

1. REPORT DATE *(DD-MM-YYYY)*	2. REPORT TYPE	3. DATES COVERED *(From - To)*
00-06-2016	Final Technical Report	04/28/2011 - 08/31/2015

4. TITLE AND SUBTITLE
Neutralization of Aerosolized Bio-agents by Filled Nanocomposite Materials through Thermal and Chemical Inactivation Mechanisms

5a. CONTRACT NUMBER
HDTRA1-11-1-0017

5b. GRANT NUMBER

5c. PROGRAM ELEMENT NUMBER

6. AUTHOR(S)
Grinshpun, S.A., Adhikari, A., Reponen, T., Dreizin, E., Schoenitz, M.

5d. PROJECT NUMBER

5e. TASK NUMBER

5f. WORK UNIT NUMBER

7. PERFORMING ORGANIZATION NAME(S) AND ADDRESS(ES)
University of Cincinnati, Cincinnati, OH 45267
New Jersey Institute of Technology, Newark, NJ 07102

8. PERFORMING ORGANIZATION REPORT NUMBER

9. SPONSORING/MONITORING AGENCY NAME(S) AND ADDRESS(ES)
Defense Threat Reduction Agency
8725 John J. Kingman Road
Fort Belvoir, VA 22060-6201

10. SPONSOR/MONITOR'S ACRONYM(S)
DTRA

11. SPONSOR/MONITOR'S REPORT NUMBER(S)
DTRA-TR-16-68

12. DISTRIBUTION/AVAILABILITY STATEMENT
Distribution Statement A. Distribution Statement A. Approved for public release; distribution is unlimited.

13. SUPPLEMENTARY NOTES

14. ABSTRACT
The main objective of the grant was to develop and characterize new materials that are useful as energetic components while releasing highly potent biocidal combustion products. These materials are intended to replace or supplement metal fuel powders in the current energetic formulations. The goal is to make them stable, easy to handle, and compatible with the other formulation components. Beyond the material development and characterization scope, this study aimed at extensively testing the biocidal efficiency of the newly-prepared compositions against stress-resistant aerosolized bacterial endospores serving as surrogates for Bacillus anthracis.

15. SUBJECT TERMS
Bio-agent, inactivation, spores, combustion, reactive materials.

16. SECURITY CLASSIFICATION OF:			17. LIMITATION OF ABSTRACT	18. NUMBER OF PAGES	19a. NAME OF RESPONSIBLE PERSON
a. REPORT	b. ABSTRACT	c. THIS PAGE			Allen Dalton
U	U	U	UU	43	19b. TELEPHONE NUMBER *(Include area code)* 703-767-3054

UNIT CONVERSION TABLE

U.S. customary units to and from international units of measurement*

U.S. Customary Units	Multiply by → / ← Divide by†		International Units
Length/Area/Volume			
inch (in)	2.54	$\times 10^{-2}$	meter (m)
foot (ft)	3.048	$\times 10^{-1}$	meter (m)
yard (yd)	9.144	$\times 10^{-1}$	meter (m)
mile (mi, international)	1.609 344	$\times 10^{3}$	meter (m)
mile (nmi, nautical, U.S.)	1.852	$\times 10^{3}$	meter (m)
barn (b)	1	$\times 10^{-28}$	square meter (m^2)
gallon (gal, U.S. liquid)	3.785 412	$\times 10^{-3}$	cubic meter (m^3)
cubic foot (ft^3)	2.831 685	$\times 10^{-2}$	cubic meter (m^3)
Mass/Density			
pound (lb)	4.535 924	$\times 10^{-1}$	kilogram (kg)
unified atomic mass unit (amu)	1.660 539	$\times 10^{-27}$	kilogram (kg)
pound-mass per cubic foot (lb ft^{-3})	1.601 846	$\times 10^{1}$	kilogram per cubic meter (kg m^{-3})
pound-force (lbf avoirdupois)	4.448 222		newton (N)
Energy/Work/Power			
electron volt (eV)	1.602 177	$\times 10^{-19}$	joule (J)
erg	1	$\times 10^{-7}$	joule (J)
kiloton (kt) (TNT equivalent)	4.184	$\times 10^{12}$	joule (J)
British thermal unit (Btu) (thermochemical)	1.054 350	$\times 10^{3}$	joule (J)
foot-pound-force (ft lbf)	1.355 818		joule (J)
calorie (cal) (thermochemical)	4.184		joule (J)
Pressure			
atmosphere (atm)	1.013 250	$\times 10^{5}$	pascal (Pa)
pound force per square inch (psi)	6.984 757	$\times 10^{3}$	pascal (Pa)
Temperature			
degree Fahrenheit (^oF)	$[T(^oF) - 32]/1.8$		degree Celsius (^oC)
degree Fahrenheit (^oF)	$[T(^oF) + 459.67]/1.8$		kelvin (K)
Radiation			
curie (Ci) [activity of radionuclides]	3.7	$\times 10^{10}$	per second (s^{-1}) [becquerel (Bq)]
roentgen (R) [air exposure]	2.579 760	$\times 10^{-4}$	coulomb per kilogram (C kg^{-1})
rad [absorbed dose]	1	$\times 10^{-2}$	joule per kilogram (J kg^{-1}) [gray (Gy)]
rem [equivalent and effective dose]	1	$\times 10^{-2}$	joule per kilogram (J kg^{-1}) [sievert (Sv)]

*Specific details regarding the implementation of SI units may be viewed at http://www.bipm.org/en/si/.

†Multiply the U.S. customary unit by the factor to get the international unit. Divide the international unit by the factor to get the U.S. customary unit.

Grant/Award #:	**HDTRA1-11-1-0017**
PI Name:	**Sergey A. Grinshpun, PhD, Professor**
Organization/Institution:	**University of Cincinnati**
Project Title:	**Neutralization of Aerosolized Bio-agents by Filled Nanocomposite Materials through Thermal and Chemical Inactivation Mechanisms**

What are the major goals of the project?

The main objective of the grant was to develop and characterize new filled nanocomposite materials (FNMs) that are useful as energetic components while releasing highly potent biocidal combustion products. These materials were intended to replace or supplement metal fuel powders in the current energetic formulations. The goal is to make them stable, easy to handle, and compatible with the other formulation components. Beyond the material development and characterization scope, this study aimed at extensively testing the biocidal efficiency of the newly-prepared compositions against stress-resistant aerosolized bacterial endospores serving as surrogates for *Bacillus anthracis*, specifically Bt(k) and BG spores. The quantitative assessment of the spore inactivation by combusting FNMs requires differentiating the heat-induced stress from the "chemical" stress, which required developing/adopting appropriate experimental methods and facilities for assessing the inactivation of aerosolized spores in well-characterized, temperature-uniform microenvironments with variable time of exposure (~100 ms to ~2 s) to gaseous biocidal compounds, such as iodine, released in the process of powder combustion of the newly-developed materials. The project activities can be broken down according to the following two research directions:

1. Preparation and optimization of new biocidal reactive materials; characterization of combustion mechanisms of biocidal reactive materials; characterization of aging of biocidal reactive materials;

and

2. Evaluation of biocidal effectiveness of the prepared materials; exploration of mechanisms responsible for the observed biocidal effects (including thermal and chemical factors affecting the spore inactivation.

The ultimate goal remains to achieve stable and aging-resistant materials capable of inactivating viable *Bacillus anthracis* (B.a.) spores while showing the combustion performance as good as or better than that of pure Al powders.

What was accomplished under these goals?

1. Preparation, characterization and optimization of newly-developed materials

1.1. Aluminum-Iodoform Composite Reactive Material

1.1.1. Previous work

There is substantial interest in reactive materials with biocidal combustion products capable of eliminating or inactivating aerosolized microorganisms (Sullivan et al., 2013; Johnson et al., 2013; Zhang et al., 2012; Grinshpun et al., 2012; Sullivan et al., 2011; Farley et al., 2010). Research has primarily addressed fuels and oxidizers modified by added halogens, although additives including other materials with known biocidal properties were also investigated. Some of the specific materials prepared and tested include silver oxides, iodine oxides, and thermite systems with silver iodates (Sullivan et al., 2013; Sullivan et al., 2015; Jian et al., 2012; Christe et a., 2010).

Generally, it is possible to classify different reactive materials capable of producing biocidal combustion products in three main groups:

- Fuels, such as aluminum based powders (Zhang et al., 2012; Zhang et al., 2010a; Grinshpun et al., 2010);
- Oxidizers, such as iodine oxides or iodate-based compositions (Christe et al; 2013);
- Energetic formulations, such as thermites containing both fuel and oxidizer, with at least one of the components producing biocidal products (Sullivan et al., 2013; Johnson et al., 2013; Farley et al., 2010; Sullivan et al., 2011);
- For either fuels or oxidizers to be used as drop-in replacements in the current energetic formulations, they should be compatible with the other formulation components and sufficiently stable to endure conventional processing routine. (Badgujar et al., 2008; Agrawal, 2005) Use of the reactive materials comprising both fuel and oxidizer may require a complete redesign of energetic formulations. In any case, stability, compatibility with common binders, and insensitivity to ignition, e.g., by spark, are critical practical characteristics required of new reactive materials.

Both silver oxide and iodine oxides are expected to yield large quantities of biocidal combustion products; however they are moisture sensitive and relatively hard to handle. In initial experiments with silver oxide, the desired elemental silver, known to be a biocide, was not produced during combustion (Sullivan et al., 2013). Most of the currently tested thermite compositions include moisture-sensitive oxides and nano-powders, such as nano-Al, known to be very sensitive to spark ignition (Azhagurajan et al., 2012; Doorenbos et al., 2009; Bulian et al., 2008).

Conversely, metal-halogen powders prepared by mechanical alloying with high energy densities, comparable to pure aluminum, are relatively stable and insensitive, and produce effective biocidal combustion products (Zhang et al., 2012; Zhang et al., 2010a; Zhang et al., 2010b; Dreizin et al., 2011). Previous work investigated mechanically alloyed composites, $Al{\cdot}I_2$ (Zhang et al., 2012; Zhang et al., 2010a; Zhang et al., 2010b) and $Al{\cdot}B{\cdot}I_2$ (Dreizin et al., 2011), prepared by ball milling elemental iodine respectively with aluminum and with blended

aluminum/boron powders. Although these materials were shown to be effective in inactivating aerosolized microorganisms (Grinshpun et al., 2012; 2012a), elemental iodine used for their preparation is relatively unstable and quite volatile under ambient conditions with vapor pressure of 0.041 kPa at 298 K (Gillespie et al.,1936). This work, therefore, is aimed to prepare stable aluminum-based iodine-containing powders without use of elemental iodine as a starting material. In particular, iodoform, CHI_3, which is a more stable iodine carrier with vapor pressure of 0.005 kPa at 298 K (Shemer et al. 2005) is explored. In addition to iodine, iodoform contains carbon and hydrogen, which are both known to be effective fuels and may result in an improvement of energetic characteristics of the mechanically alloyed powders.

Iodoform is widely used in medicine as an antiseptic and antimicrobial agent. It is much less volatile and more stable at ambient conditions compared to elemental iodine. The sublimation of iodoform begins around 80 °C and the melting is reported to occur around 120 °C (Bieliński et al., 2007). When exposed to higher temperatures, iodoform starts to decompose around 160 °C, and major decomposition products include double-ionized iodine, iodine radical, and oxidation products of CHI_3 or iodine (e.g. HIO_3) (Bieliński et al., 2007). While Al-based composites using elemental iodine are best milled at liquid nitrogen temperature, so that iodine is solidified, this requirement may be less stringent for iodoform, and both room temperature and cryo-milling options can be explored for preparation of aluminum-based, iodine containing powders.

1.1.1. Experimental

The starting material were aluminum powder, -325 mesh size (<45 μm), 99.5% pure, from Atlantic Equipment Engineers, and iodoform powder, purchased from Alfa Aesar, 99% pure.

1.1.1.1. Ball-milling equipment and parameters

Two different ball-mills were used to prepare mechanically alloyed powders at room temperature and at the temperature of liquid nitrogen (-196 °C). A model 01HD attritor mill by Union Process with the vial cooled by liquid nitrogen, and a shaker mill (SPEX Certiprep, 8000 series) with the vial cooled by an air jet at room temperature were used to prepare composite samples A and B, respectively. The starting materials, Al and CHI_3, were mixed to obtain a material composition with a mass ratio of Al/I = 80/20 for both samples, to be directly comparable with the $Al{\cdot}I_2$ composites investigated earlier (Grinshpun et al., 2012). Both materials were milled using 3/8”-diameter case-hardened carbon steel balls.

Sample A prepared by cryogenic milling produced a 50-g batch of powder. It was prepared in a 750 mL stationary stainless steel milling vial placed inside an insulated cooling jacket, through which liquid nitrogen was circulated at approximately 2 CFM (0.94 L/s). The ball to powder mass ratio was 36. An impeller rotated at 400 rpm and the milling time was 24 hours. Additional information regarding the cryogenic milling process in the attritor mill is provided elsewhere (Zhang et al., 2010b). Sample B synthesized by milling at room temperature was prepared in two 50-mL flat-ended steel vials simultaneously. Each vial contained 5 g of powder. Ball to powder mass ratio was 10. The vials were loaded and sealed inside an argon-filled glovebox. The milling time was 8 hours.

Milling parameters are summarized in Table 1.1.1.

Table 1.1.1. Milling parameters

Sample ID	Milling Media	Milling Time (hrs)	Batch Size (g)	BPR	Milling Condition
A	Attritor Mill	24	50	36	cryogenic
B	Shaker Mill	8	5	10	ambient

1.1.1.2. Characterization techniques and instrumentation

Back-scattered scanning electron microscopy (SEM) images were used to characterize the morphologies of both samples. Particle size distribution (PSD) of each sample was measured with low-angle laser light scattering using a Beckman-Coulter LS230 Particle Counter. A PANalytical Empyrean diffractometer was used for X-ray diffraction (XRD) to determine phase composition for each sample. The XRD powder diffractometer was operated at 45 kV and 40 mA using unfiltered Cu K_α radiation (λ=1.5438Å).

The stability of iodoform encapsulation into the Al-matrix and the release of iodine upon heating were investigated using thermo-gravimetric (TG) analysis. Under argon gas, TG traces for iodine release were obtained using a Netzsch Simultaneous Thermal Analyzer STA409 PG with a TG sample holder. A small piece of zirconium foil was placed in the furnace below the sample hlder as an oxygen getter to eliminate any oxidation involving residual or trace oxygen. The furnace was purged with argon at 50 mL/min. The sample mass for each experiment varied in the range of 19 – 23 mg.

Oxidation of the prepared powders was studied using a TA Instruments model Q5000IR thermo-gravimetric analyzer. The powder was loaded into an alumina crucible with a sample mass of 2 – 4 mg. The balance was purged with argon at 10 mL/min and the furnace was purged with oxygen at 25 mL/min.

Ignition of the milled powder was characterized in air using a heated filament experiment described in detail elsewhere (Shoshin et al., 2006; Ward et al., 2006) A slurry with milled material and hexane was made to prepare a thin, 1-cm long coating on a 4.5 cm long, 0.5 mm diameter nickel-chromium alloy heating wire. The coated wire was heated by a DC current. Varied applied voltage and adjustable resistors connected in series with the wire were used to vary the heating rates in the range of 1000 – 10,000 K/s. The temperature of the filament was measured using a high-speed infrared pyrometer (DP1581 by Omega Engineering, Inc.) focused on an uncoated filament surface adjacent to the powder coating. The emission from the powder coating was visualized using a high speed video camera (MotionPro 500 by Redlake), operated at 500 fps. Prior to ignition, the coating surface was darker than that of the heated filament. The ignition instant was registered when the powder became brighter than the heated filament.

Combustion studies were conducted using a constant volume explosion (CVE) experiment.](Umbrajkar et al., 2008; Stamatis et al., 2009) A spherical vessel of 9.2 L was used. The vessel

was initially evacuated and the aerosolized powder was introduced into the vessel using an air blast delivered from a pressurized reservoir. The pre-ignition pressure in the vessel was close to 1 atm. After a 0.3-s delay necessary to minimize the turbulence, the powder cloud was ignited by an electrically heated tungsten wire placed at the center of the vessel. The pressure inside the vessel was recorded as function of time using a pressure transducer by Schaevitz Sensors. The ratio of the maximum pressure to the initial pressure, P_{max}/P_{ini}, and maximum rate of pressure rise, $(dP/dt)_{max}$, were identified to characterize the energy released during the experiment and the rate of combustion, respectively. The CVE experiment was conducted with a fuel-rich system at a constant powder load of 4.65 g of the composite $Al{\cdot}CHI_3$ powder. Assuming that the only combustion products are Al_2O_3, I_2O_5, CO_2, and H_2O, this powder load corresponds to an equivalence ratio of about 1.45. Present results can be directly compared to earlier experiments using the same experimental setup and pure aluminum powders, for which the same mass load was used to achieve reproducible ignition. (Zhang et al., 2012)

1.1.2. Results

1.1.2.1. Particle sizes, morphology, and stability

After milling, both samples were recovered under argon; portions of the powders were loaded in clear glass bottles and stored under ambient condition. The glass bottles were closed but not sealed; thus, the powder was slowly exposed to air as well as the humidity present in the air-conditioned laboratory air. A noticeable difference in color due to aging was seen in sample B within two weeks of storage. Originally gray colored sample B changed to yellowish-gray, indicating release of iodine and its presence on the surface of the powder. The remainder of sample B that was stored under argon did not show any discoloration. No discoloration was observed for sample A stored in room air. These initial observations show that the cryogenic milling conditions help stabilize the iodoform in the Al-matrix.

SEM images of the samples A and B (cf. Table 1.1.1) are shown in Fig. 1.1.1. The milled powders contain equiaxial particles with many fines (particles less than 10 μm.) Qualitatively, it appears that sample B includes more coarse particles compared to sample A. The images were produced using backscattered electrons; thus, they were sensitive to the phase contrast between elements with different atomic weights. For both samples, particle surfaces appear to be homogeneous and phase contrast is not detectable despite a large difference in the atomic weight of iodine and aluminum, which was expected to result in substantially brighter surfaces rich with iodoform. The uniform surface brightness indicates a homogeneous distribution of iodoform in the prepared composite powders.

The particle size distribution (PSD) and respective volume mean particle sizes for both samples A and B are presented in Fig. 1.1.2. The average particle sizes are 14.1 μm and 26.0 μm for samples A and B, respectively. It is observed, therefore, that the milling at cryogenic temperatures (sample A) helps achieving finer particle sizes. It appears that for both samples the size distributions are bimodal; for sample A the second peak is relatively well resolved whereas for sample B it appears as a shoulder at the coarse-particle side of the distribution curve.

The XRD patterns for both samples are shown in Fig. 1.1.3, where all the observed intensity peaks represent pure aluminum. There are no clear differences between the XRD patterns for both samples.

Surface area of sample A was measured to be 4.50 m^2/g, using Brunauer, Emmett and Teller (BET) method with MONOSORB® surface area analyzer manufactured by Quantachrome Corp. The high surface area may be the result of particles having well developed rugged surface with small crevices observed from the image in Fig. 1.1.1. The measurements were not performed for sample B which was difficult to handle in open air.

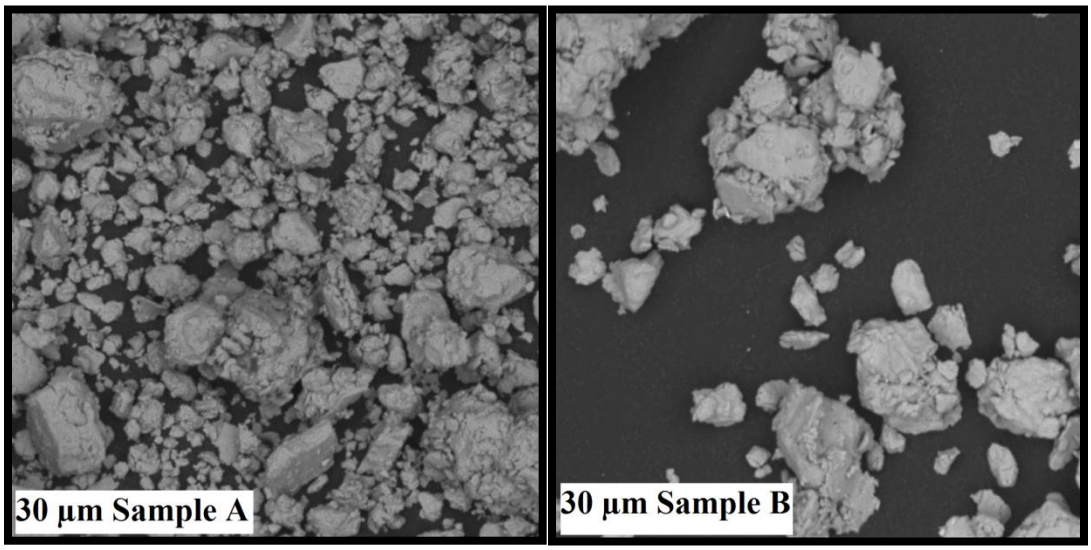

Fig. 1.1.1. SEM images of sample A and sample B.

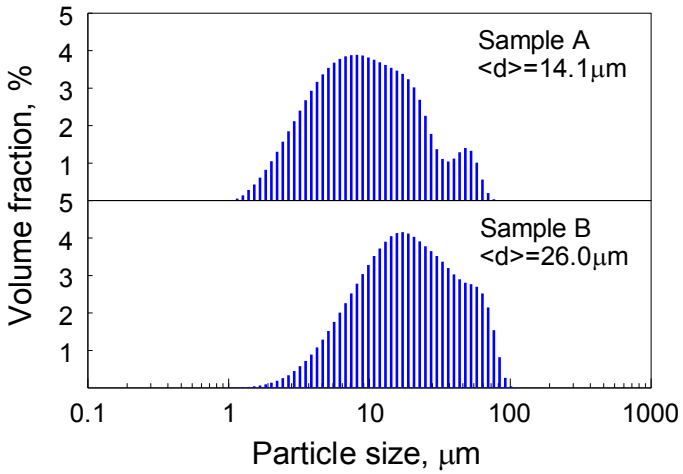

Fig. 1.1.2. Particle size distribution of milled sample A and sample B.

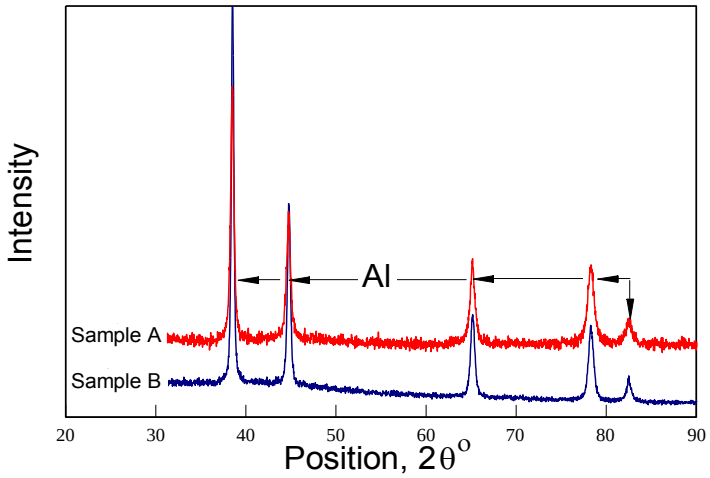

Fig. 1.1.3. XRD patterns of sample A and sample B

1.1.2.2. Iodine release

For sample A, heating rates were varied from 2 to 20 K/min and experiments were carried out to the maximum temperature of 1400 °C. Derivatives of the TG traces, dm/dT, were used to identify individual stages of iodine release occurring during the temperature ramp. Both TG traces and their derivatives are shown in Fig. 1.1.4. For reference, a single TG trace recorded at 10 K/min is also shown for Al·I_2. (Zhang et al., 2012) Qualitatively, iodine release for the prepared Al-iodoform powder is similar to that observed for Al·I_2.

The minima of the derivatives of TG traces show peaks in the rates of mass loss. There were four distinguishable peaks, and, respectively, four iodine release stages could be identified for sample A at heating rates of 10 K/min and above. The derivative peaks for stages I, II and IV show a shift towards higher temperatures with increasing heating rates, while the peak for stage III remains at an effectively constant temperature. At heating rates of 2 and 5 K/min, stages III and IV overlap, and only at higher heating rates does the peak for stage IV shift sufficiently to distinguish it from the stage III peak.

For sample B, because of its poor stability, a TG trace was recorded only at one heating rate of 20 K/min, as illustrated in Fig. 1.1.5. Based on the TG derivative trace, two iodine release stages could be distinguished.

The iodine release stages for samples A and B could be compared to each other semi-quantitatively considering TG traces recorded at 20 K/min for both samples. This comparison is presented Table 1.1.2. Note that stages I and II are not the same for samples A and B, based on their respective temperature ranges. Stage II for sample B can roughly be related to stages III and IV for sample A.

For sample A, the iodine release at low-temperature stages I and II is quite small. Most of iodine is released in the vicinity of the aluminum melting point. Conversely, sample B shows a significant amount of sample mass loss (14.7%) during its low-temperature stage I.

These results show that the iodoform is much better stabilized inside the Al-matrix for sample A compared to sample B. This is consistent with the qualitative observation of discoloration/aging for sample B.

Because of poor stability of sample B, it was not characterized further.

Table 1.1.2. Iodine release stages at 20 K/min for sample A and B.

Sample ID		*stage I*	*stage II*	*stage III*	*stage IV*
A	Temp Range (°C)	104 - 301	407 – 513	543 - 693	693 – 786
	Δ Total Mass (%)	-2.4	-5.4	-12.1	-18.1
B	Temp Range (°C)	80 - 456	566 – 781		
	Δ Total Mass (%)	-14.7	-20.1		

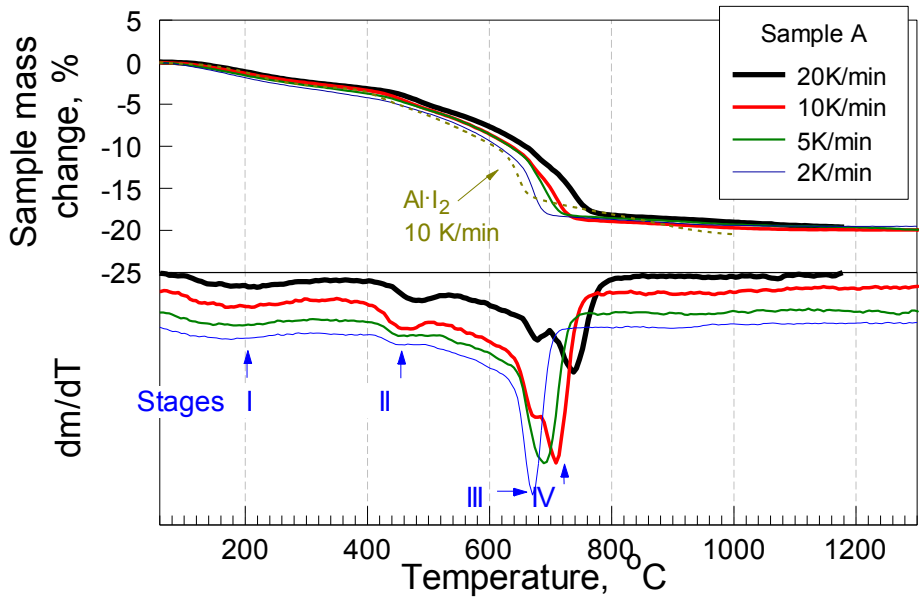

Fig. 1.1.4. Mass change and derivative traces for sample A in heated in argon at various heating rates.

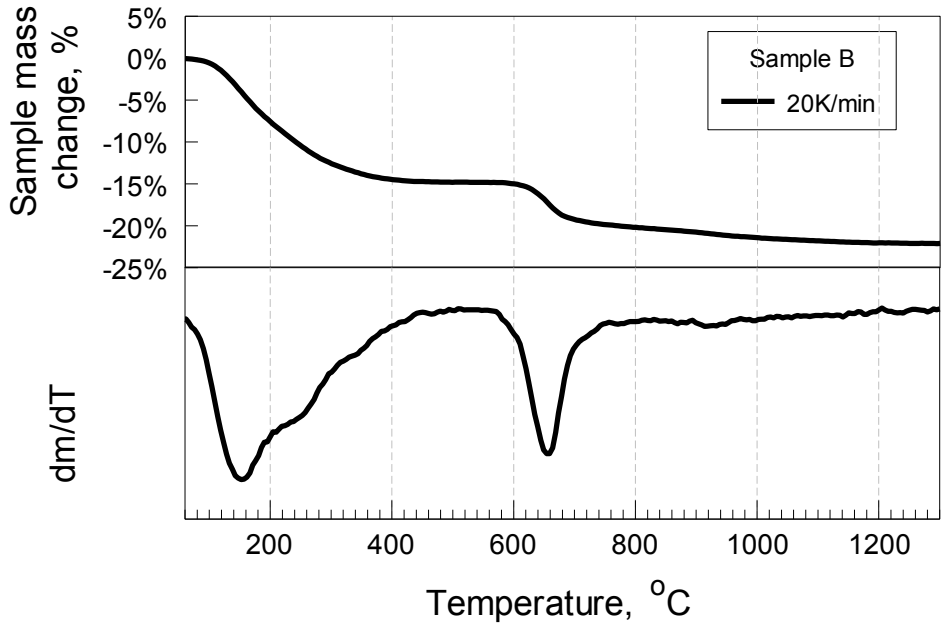

Fig. 1.1.5. Mass change and derivative traces for sample B heated in argon at 20 K/min.

1.1.2.3. Oxidation

The oxidation of sample A was studied using heating rates from 2 to 20 K/min and the results are presented in Fig. 1.1.6. Once again, for reference, a TG trace for oxidation of Al·I_2 heated at 10 K/min is shown (Zhang et al., 2012). Qualitatively, oxidation behavior of sample A is similar to that of Al·I_2. However, sample A oxidizes somewhat faster than Al·I_2; also, a small stepwise mass increase is clearly observed for sample A when Al melts while it is less noticeable for Al·I_2.

The TG traces for the Al-iodoform composite (sample A) show initial mass loss at low temperatures corresponding to release of iodine before two sharp oxidation steps are observed. As expected for thermally activated processes, higher heating rates result in a shift of the oxidation steps to higher temperatures.

The magnitude of the first oxidation step appears to be smaller for lower heating rates, compared to the higher heating rate experiments. The overall mass gain (and thus, the oxidation degree) remains quite consistent when the material is heated to 1000 °C at different heating rates.

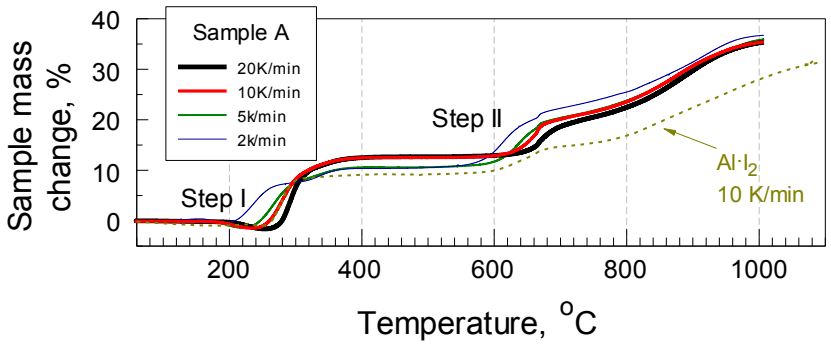

Fig. 1.1.6. Oxidation of sample A at various heating rates.

1.1.2.4. Ignition

Figure 1.1.6 shows the measured ignition temperatures for sample A as a function of the heating rate. The data are scattered in a relatively narrow range of temperatures. A very weak trend of increasing temperatures at greater heating rates may be observed.

For comparison, ignition temperatures of Al·I_2 powder are also shown in Fig. 1.1.7. It is apparent that Al-iodoform ignites at substantially lower temperatures than Al·I_2

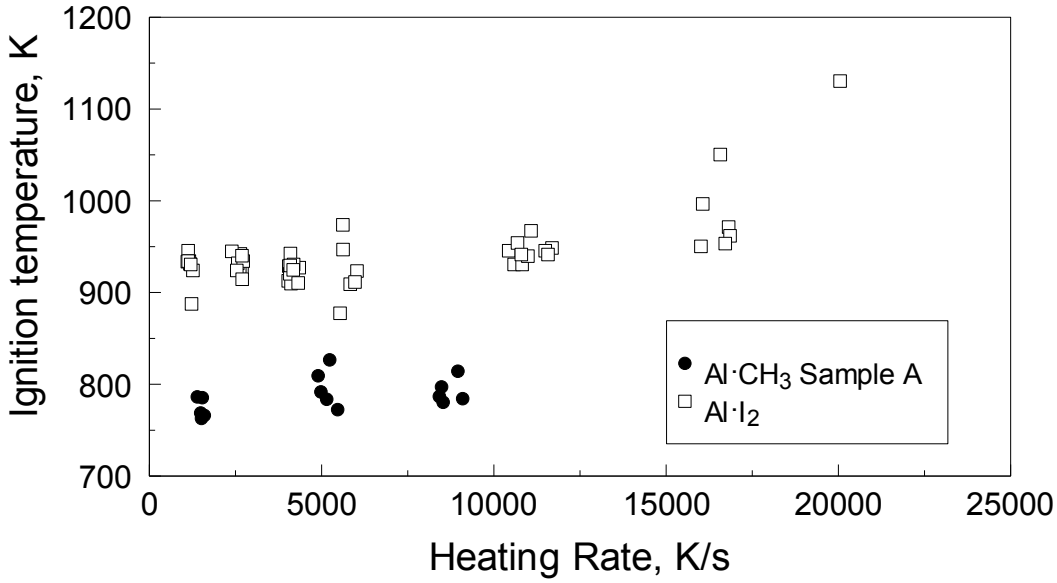

Fig. 1.1.7. Ignition temperature of sample A and Al·I_2 composite at different heating rates in air

1.1.2.5. Reaction Kinetics

Temperatures marking positions of individual stages of iodine release (minima in the TG derivative traces), oxidation steps, and ignition temperatures are shown in a Kissinger plot (Starink, 2003) in Fig. 1.1.8. The vertical axis shows $\ln(T^2/\beta)$, where β is the heating rate and T

is the specific event temperature; the horizontal axis is the reciprocal temperature, 1/T. Iodine release stages I and II do not correlate with the first oxidation step. In contrast, the iodine release stages III and IV correlate with the second oxidation step occurring near the Al melting point.

Comparing events observed in low-heating rate TG experiments with ignition, it becomes apparent that ignition is well correlated with the iodine release stage II. Extrapolation of the kinetic trend for the first oxidation step into high heating rates also points to the temperature range close to that observed for ignition; however, the effect of heating rate on oxidation during stage I appears to be noticeably stronger than that observed for ignition temperatures.

Activation energies, ΔE, of individual iodine release stages and oxidation steps are directly proportional to the slopes of the linear-regression line that can be obtained from the Kissinger plot shown in Fig. 1.1.8. No activation energy value is shown for the iodine release stage III, which appears to directly correlate with the Al melting. The activation energies are presented and compared to those for $Al{\cdot}I_2$ in Table 1.1.3. Although TG traces for both $Al{\cdot}CHI_3$ and $Al{\cdot}I_2$ look qualitatively similar to each other, a difference in activation energies for both individual iodine release stages and oxidation steps is observed. Activation energies of iodine release are generally lower for $Al{\cdot}CHI_3$. If the decomposition rate is limited by diffusion, then this lower activation barrier suggests lower diffusion resistance in the case of the iodoform composite, possibly due to particle disintegration and therefore increased creation of new surface during decomposition

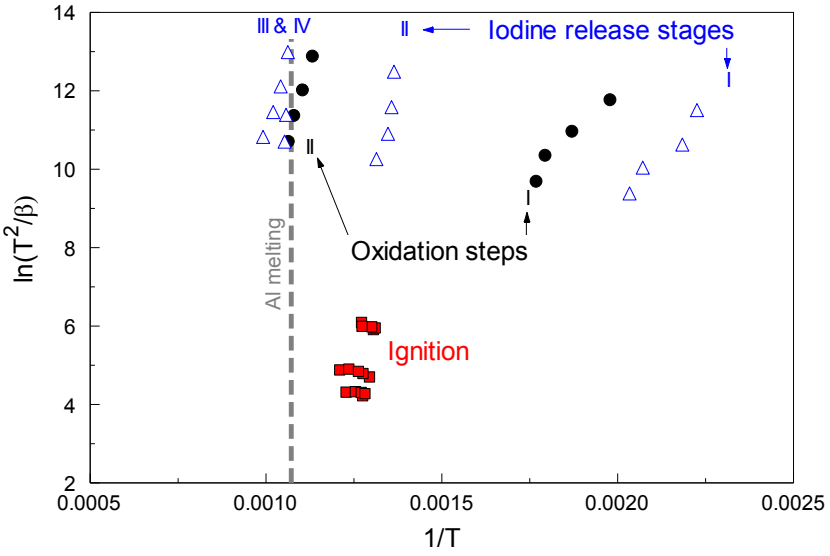

Fig. 1.1.8. Kissinger plot of sample A with ignition temperatures (squares), iodine release stages (triangles), and oxidation steps (circles) measured at different heating rates. Al melting point (dashed line) is also shown.

For oxidation, the activation energies for the first step are similar for both $Al{\cdot}I_2$ and $Al{\cdot}CHI_3$. For the second step, activation energy for $Al{\cdot}CHI_3$ is lower.

Table 1.1.3. Activation energies, ΔE (kJ/mol), for Al·CHI$_3$ and Al·I$_2$ for various kinetic mechanisms

	Iodine release			*Oxidation*	
	stage I	stage II[a]	stage IV[a]	step I	step II
Al·CHI$_3$	80±15	330±110	250±30	76±12	260±15
Al·I$_2$	130±10	530±100	530±90	65±6	380±39

[a] In the referred study, the iodine release stages corresponding to stages II and IV for Al·I$_2$ are referred to as "additional" and stage II, respectively.

1.1.2.6. Combustion

Sample A ignited readily inside the explosion vessel; an example of characteristic pressure traces is shown in Fig. 1.1.9. A summary of results is given in Fig. 1.1.10. The results include the average ratios of maximum explosion pressure, P_{max}, to the initial pressure, P_{ini} and the average maximum rate of pressure rise, $(dP/dt)_{max}$ for sample A compared to those for Al·I$_2$ and several reference aluminum powders with volume-based average particle sizes varied from 9.0 to 15.1 μm. From earlier work (Umbrajkar et al.,2008; Stamatis et al.,2009 Santhanam et al; 2010); P_{max}/P_{ini} and $(dP/dt)_{max}$ are known to be proportional to the flame temperature and combustion rate, respectively. In comparison to the reference aluminum powder, sample A has higher values of both P_{max}/P_{ini} and $(dP/dt)_{max}$. Combustion characteristics for the prepared Al·CHI$_3$ composite are similar to those observed for Al·I$_2$ (Zhang et al., 2012)

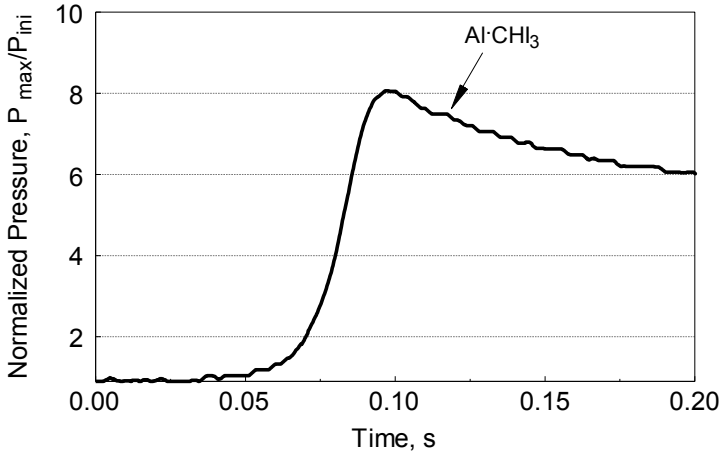

Fig. 1.1.9. A characteristic pressure trace recorded in CVE experiments with the prepared Al·CHI$_3$ composite powder burning in air (sample A).

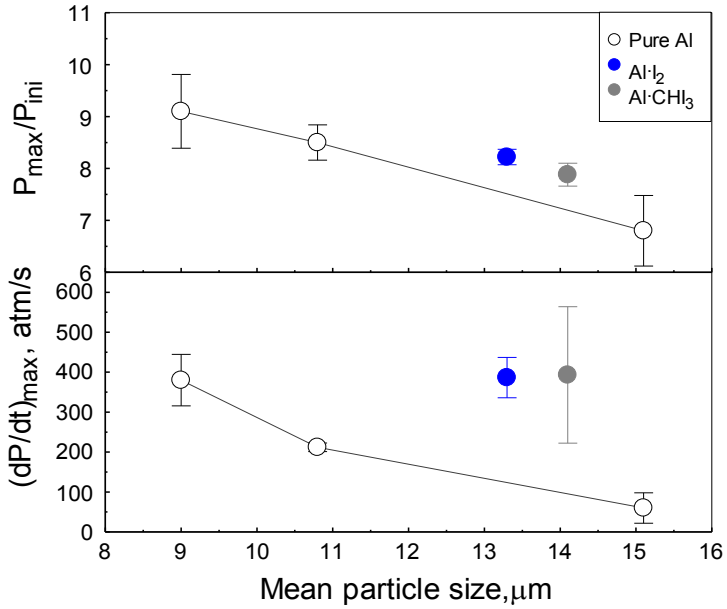

Fig. 1.1.10. Comparison of CVE experiment results, maximum pressure and rate of pressure rise, for pure aluminum, $Al{\cdot}I_2$, and the prepared $Al{\cdot}CHI_3$ composite powder (sample A.)

Because the prepared powder is substantially different from pure aluminum, a more useful assessment of its combustion effectiveness compared to aluminum may be obtained considering results of respective thermodynamic equilibrium calculations. The calculations were performed using NASA CEA code (McBride et al., 1996). Constant volume combustion was considered for two cases: aluminum/air and aluminum/iodoform/air. The calculations were performed for different powder mass loads and accounting for the experimental chamber volume. The maximum powder mass used in calculations corresponded to the experimental load. Smaller powder loads were considered to account for situations that are likely to occur in experiments: some of the powder may not be effectively aerosolized and remain in the reservoir even after the air blast; in addition, some of the aerosolized powder could be deposited onto the explosion chamber walls before ignition. Previous experience suggests that the correction of the powder mass may be as large as 20%. (Eapen et al., 2004)

The results in terms of for P_{max}/P_{ini} and T_{max} are shown in Fig. 1.1.11.

The flame temperature for the aluminum/air mixture peaks at about 3 g mass load. For the iodoform-containing mixture, the peak temperature is observed at a greater powder load, close to 3.75 g, whereas the mass of aluminum as a component in the aluminum-iodoform powder remains close to 3 g. The peak temperature for the iodoform-containing mixture is somewhat lower than for the pure aluminum combustion.

Generally, the calculated pressure ratios, P_{max}/P_{ini}, tend to increase with increasing powder mass for both fuels. The trend is stronger for the iodoform-containing mixture. The pressure is clearly affected by both calculated temperatures and product species and for the experimental powder load, 4.65 g, the equilibrium pressure is expected to be higher for the iodoform-containing

powder. However, this situation reverses for lower powder loads, which can be more relevant for the experimental conditions, when powder losses may occur during dispersion and on the vessel walls.

Because the range of powder mass loads shown in Fig. 1.1.11 is likely greater than possible variation in the sample mass in experiments due to all possible losses, one observes that the range of pressure changes, is less than 5% for the iodoform-containing mixture and even narrower than that for the aluminum/air system. Thus, combustion efficiency of different mixtures can be relatively well assessed by direct comparison of their measured pressure ratios.

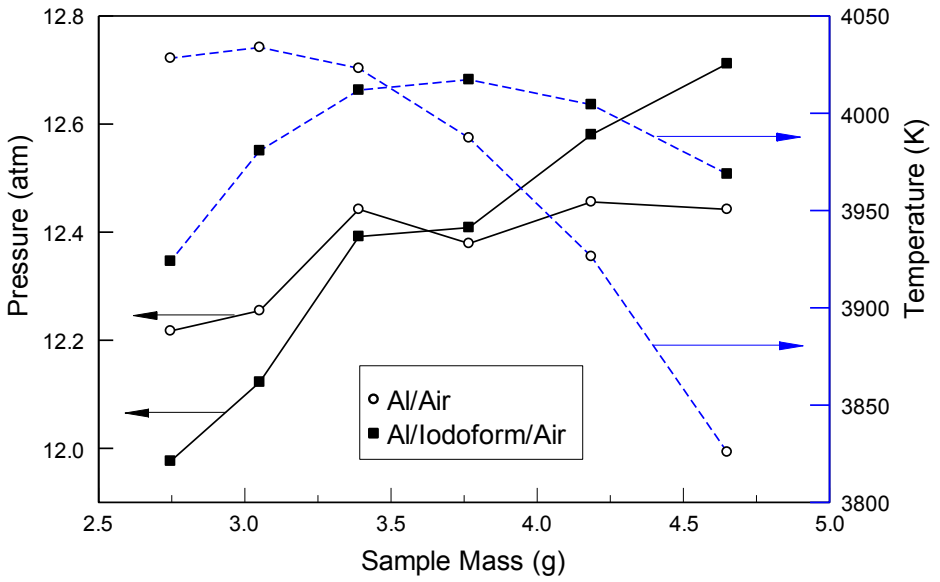

Fig. 1.1.11. CEA pressure and temperature at various theoretical sample masses

1.1.3. Discussion

1.1.3.1. Iodine release, oxidation and ignition

Samples A and B, prepared using cryo-milling and room temperature milling, respectively, illustrate the importance of milling temperature for achieving a stable composite. Although iodoform itself is relatively stable at room temperature, the stability of the Al·CHI_3 composite is substantially improved by cryo-milling (cf. Figs. 1.1.4 and 1.1.5). A relative measure of material stability, *S*, introduced for Al·I_2 composite (Zhang et al., 2012) is used to compare the stability of Al·CHI_3 to Al·I_2 and Al·B·I_2. The parameter *S* was defined as the percentage of weight loss at temperatures exceeding 400 °C (673 K). The values of S are 83% for both Al·CHI_3 (sample A) and Al·I_2 whereas for Al·B·I_2, it is 85%. Thus, both Al·CHI_3 and Al·I_2 prepared by cryo-milling are similar in stability to each other, and slightly less stable compared to Al·B·I_2.

A direct comparison of TG traces for sample A and $Al{\cdot}I_2$ shows the iodine release stages for the cryo-milling prepared $Al{\cdot}CHI_3$ are similar to those for $Al{\cdot}I_2$. Individual iodine release stages observed in the TG traces can be attributed to different ways the iodoform may be bound inside the Al-matrix. Similar to that of $Al{\cdot}I_2$ composite (Zhang et al., 2010a), the loosely bound iodoform is released from the Al-matrix during stages I and II, corresponding to the decomposition of iodoform and dissociation of AlI_3, respectively. Although pure AlI_3 boils off completely around 400 °C (Zhang et al., 2010b), the decomposition TG trace of sample A at the heating rate of 20 K/min shows the iodine release stage II spanning over the temperature range of 407 – 513 °C. Due to the encapsulation of AlI_3 in the Al matrix, its effective boiling point may be shifting to higher temperatures because most of the AlI_3 molecules may not be readily available at the sample surface to be removed. In stages III and IV, a significant amount of iodine is released around the aluminum melting point, 660 °C, indicating that iodine was confined within the aluminum crystal lattice or its defects, which are destroyed during melting. A comparison of TG traces for sample A and for $Al{\cdot}I_2$ shows that the mass of iodine stabilized in the Al-matrix is the same for both composites.

Qualitatively, both iodine release and oxidation processes are similar to those for $Al{\cdot}I_2$; however, there are differences in specific details and apparent activation energies for individual iodine release stages and oxidation steps. The lower activation energies for all iodine release stages suggest an easier release of iodine upon heating, when it is introduced by milling aluminum with iodoform. At the same time, the main sequence identified in ref. 3 and including sequential release of iodine from phases behaving as elemental iodine and as decomposing AlI_3 remains valid.

The oxidation steps for $Al{\cdot}I_2$ and $Al{\cdot}CHI_3$ are very similar to each other. However, the activation energy for the second oxidations step is noticeably lower for $Al{\cdot}CHI_3$. This might be explained by release of hydrocarbon species, resulting in a stronger disruption of the powder particle surface and thus assisting in formation of fresh surface prone to rapid oxidation.

It is important to realize that because of the difference in activation energies of different oxidation steps and iodine release stages, the order of events might be reversed at high heating rates, typical of ignition. At low heating rates, oxidation step 1 for $Al{\cdot}CHI_3$ occurs before the iodine release stage II. At high heating rates, this could no longer be the case. A linear extrapolation of the kinetic trends (Fig. 1.1.8) over a broad range of heating rates is likely invalid, and a more detailed modeling, taking into account heat transfer processes specific for each ignition configuration, is necessary to assign which of the two processes is more likely triggering ignition of the prepared $Al{\cdot}CHI_3$ powders.

In the case of $Al{\cdot}I_2$ composite, the ignition occurs at the aluminum melting point where iodine release is substantial. Although the iodine release near the aluminum melting point remains substantial for the prepared $Al{\cdot}CHI_3$ powders, they ignite at much lower temperatures. It is suggested that the ignition temperature is reduced because of the presence of hydrogen and carbon in the prepared $Al{\cdot}CHI_3$ composite powder. At the iodine release stage II for $Al{\cdot}CHI_3$, it is possible for volatile species other than iodine, e.g., hydrocarbon molecules, to escape and oxidize, if the heating occurs in an oxidizing atmosphere. The ignition may thus be accelerated by an added heat release in the direct vicinity of the powder surface. The oxidation of the

released hydrocarbon would also occur in the TG experiments; however, the process would unlikely affect the sample mass measurement – and thus, the recorded TG traces. The oxidation products are gases, e.g. CO_2, CO, OH and/or H_2O, which would be vented away from the sample and thus would not affect the heterogeneous surface reactions on its surface.

1.1.3.2. Combustion

The combustion dynamics of $Al{\cdot}CHI_3$ is very similar to that of $Al{\cdot}I_2$ (Zhang et al., 2012), therefore, one would expect similar release of iodine-containing biocidal products during combustion. From the CVE experimental results shown in Fig. 1.1.10, the $Al{\cdot}CHI_3$ composite is shown to be more energetic over comparable size pure Al powder in terms of both maximum pressure and rate of pressure rise. The improved combustion characteristics are attractive for practical applications in advanced energetics.

The overall combustion scenario of the prepared $Al{\cdot}CHI_3$ composite powder may be affected by both its ignition and combustion characteristics. In case of a powder dispersed in a fire ball generated by a high explosive, a reduced ignition temperature would imply that the prepared particles may ignite while being exposed only to the combustion products of the high explosive, well before they can be mixed with the surrounding environment. This may be advantageous for coupling their combustion energy to sustain the propagating shock wave. However, this will also mean that much of the halogenated combustion products will be released within the fire ball, where they will not effectively interact with any viable bio-aerosol.

1.1.4. Conclusions

Cryo-milling is necessary to achieve a stable $Al{\cdot}CHI_3$ composite with the same mass of iodine stabilized as for $Al{\cdot}I_2$ into the Al-matrix. The addition of hydrocarbon e.g. C and H atoms, can alter the ignition and combustion of the $Al{\cdot}CHI_3$ composite. The iodoform is bound to the Al-matrix in three different forms and during thermal decomposition, at least three different stages of iodine release are observed. The initial oxidation step occurs at a temperature higher than the first stage of iodine release; it does not correlate directly with any of the iodine release stages. The ignition of $Al{\cdot}CHI_3$ composite occurs at a lower temperature than that of $Al{\cdot}I_2$. Based on a Kissinger plot, the kinetics trends for both first oxidation step and second stage of iodine release can be extrapolated to high heating rate at the temperature range, at which ignition is observed. A relatively weak effect of heating rate on the ignition temperature suggests its better correlation with the stage II of iodine release. A relatively low ignition temperature may be associated with release and instant oxidation of volatile species other than iodine, e.g. hydrocarbon molecules. The combustion dynamics of $Al{\cdot}CHI_3$ composite is similar to that of $Al{\cdot}I_2$ composite. Furthermore, the maximum pressure and pressure rise observed in the constant volume explosion show an improvement compared to the pure Al.

Several new compositions were identified theoretically as promising based on their enthalpy of formation, initial data on stability, and availability of components. Three compositions were

prepared and initially characterized, including $Al{\cdot}TiI_4$, $Al{\cdot}Si{\cdot}I_2$, and $Al{\cdot}NbCl_5$. Several specific compositions of $Al{\cdot}TiI_4$ and $Al{\cdot}Si{\cdot}I_2$ were prepared by mechanical milling and initially characterized. All materials were found to be unstable. $Al{\cdot}TiI_4$ composites were volatile and pyrophoric. Coating these powders with Teflon was attempted. Stability was marginally improved and pyrophoricity was reduced; however, even coated powders were difficult to handle. None of the prepared $Al{\cdot}Si{\cdot}I_2$ composites was stable; iodine was not well retained and began escaping at very low temperatures. Work further focused on a more stable $Al{\cdot}NbCl_5$ composite. Material with 74 wt% of Al and 26 wt% of $NbCl_5$ was prepared using an attritor mill operated at the liquid nitrogen temperature (77 K); milling time was 24 hours and ball to powder mass ratio (BPR) was 36. 10-mm milling balls were used. On the mole basis, this prepared material contains 3 times more halogen (chlorine) as compared to composites prepared earlier with iodine. A batch of material was Teflon-coated. Both coated and uncoated powders comprised fine equiaxial particles, as shown in Fig. 1.3.1. Average volume-based particle sizes were close to 7 μm.

Thermogravimetric (TG) measurements showed that most of chlorine is retained to the temperature above 450º C. Characteristic TG curves are shown in Fig. 1.3.2. Material exposed to room air for two weeks was substantially less stable and lost more than 10% of its weight before reaching 300 ºC. Material stored in hexane was not observed to age, preserving its initial stability.

Heated filament ignition experiments for $Al{\cdot}NbCl_5$ composite powders showed that the powders ignite between 800 and 1100 ºC when heated at the rates of 1000 – 30,000 K/s.

No distinction could be made between Teflon-coated and uncoated powders.

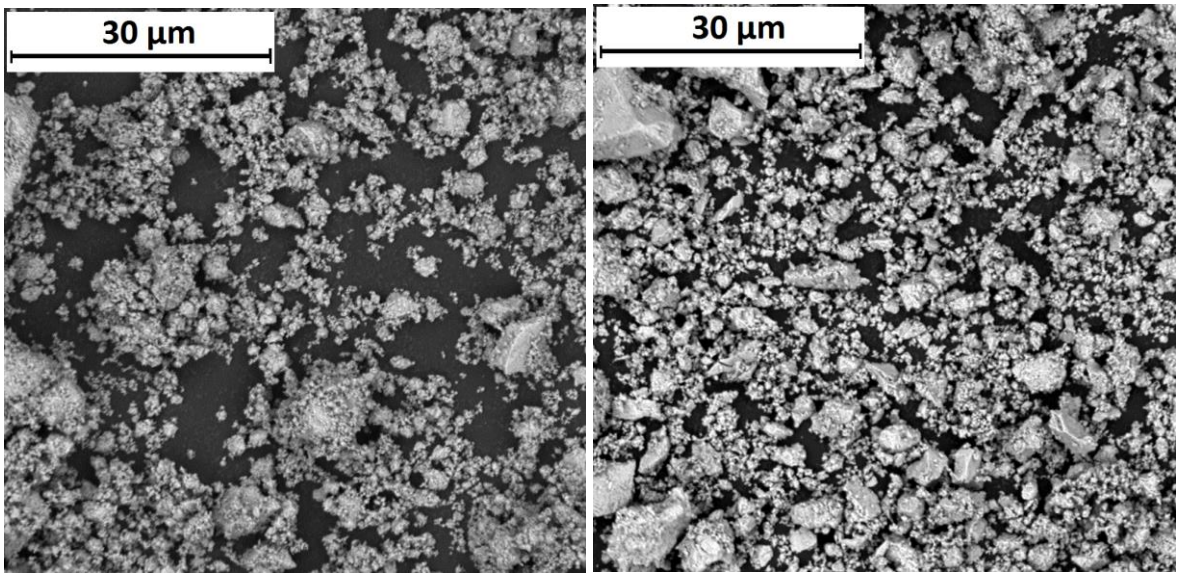

Fig. 1.3.1. Uncoated (left) and Teflon-coated (right) $Al{\cdot}NbCl_5$ composite powders prepared by cryomilling.

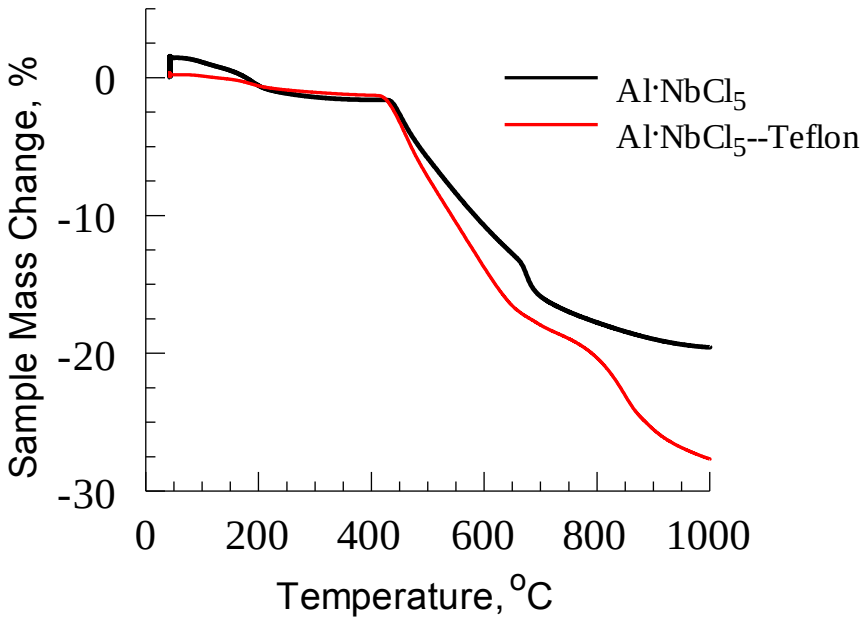

Fig. 1.3.2. TG curves for uncoated and Teflon-coated Al·$NbCl_5$ composite powders prepared by cryomilling. Heating rate 10 K/min; experiment performed in Ar flow.

Powders were injected into an air-acetylene flame and their burn times were measured optically. The burn times were compared to those for a comparably sized pure Al powder (Al X65 by Toyal America). The composite powder particles burned somewhat longer than Al particles, as shown in Fig. 1.3.3. No substantial difference in combustion behavior was observed between powders stored in air and hexane prior to the experiments.

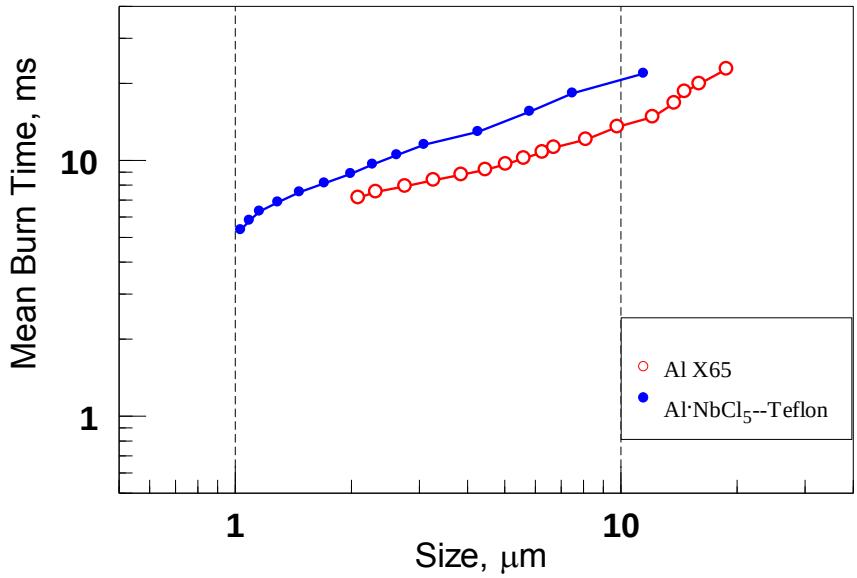

Fig. 1.3.3. Burn times of Al·$NbCl_5$ composite powder particles ignited in an air-acetylene flame. Data are compared to those for pure Al powder with comparable particle sizes.

2. Evaluation of biocidal effectiveness of newly-developed materials; exploration of inactivation mechanisms

2.1. Development and validation of the experimental set-up and protocols for evaluating the short-term inactivation of bioaerosol particles due to thermal and chemical exposures to combustion environments under uniform temperature conditions and with the time of exposure varying from ~100 ms to ~2 s.

Figure 2.1.1 below presents the principle schematics of the experimental facility that was developed and utilized in this effort for the evaluation of inactivation of aerosolized spores by different materials combusted in the burner designed and built specially for this study.

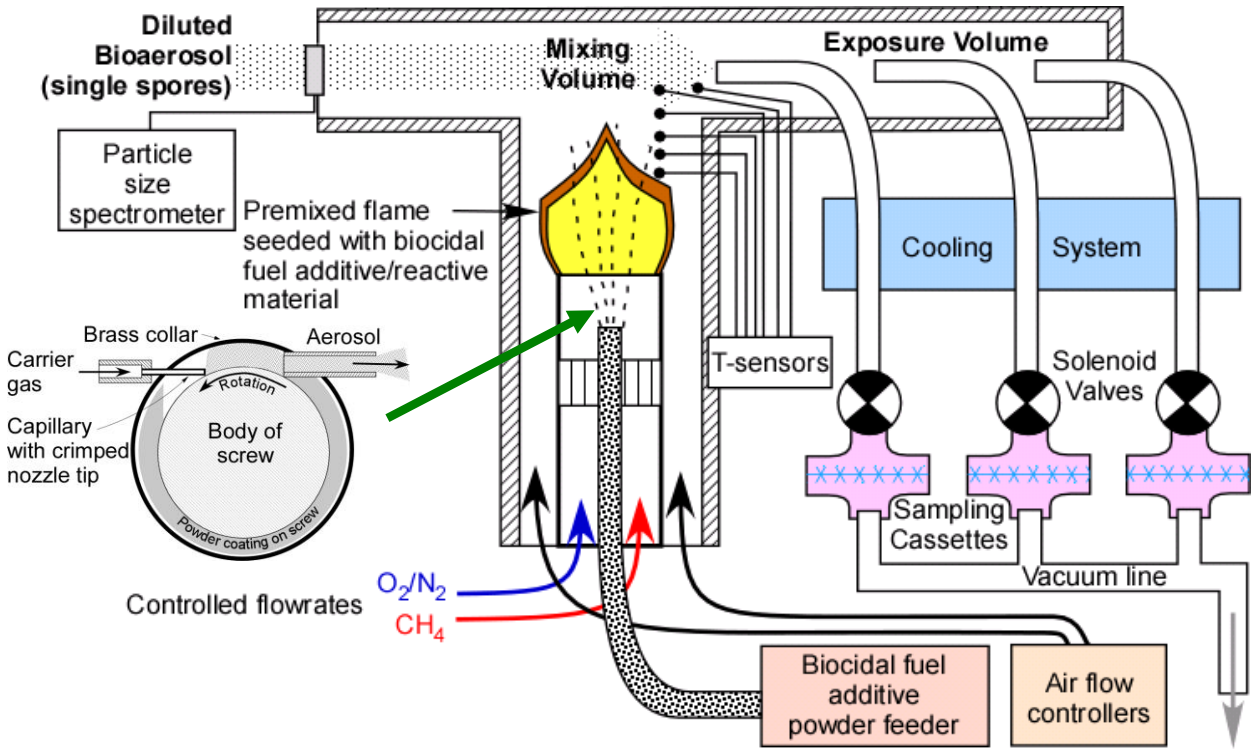

Figure 2.1.1. Experimental facility for the evaluation of inactivation of aerosolized spores.

The tested material in a powder form is fed through an air-acetylene flame. The particles ignite and burn in the combustion products of the hydrocarbon flame, while surrounding air is mixed in the combustion environment providing additional oxidizer. Initial flame and particle flow are directed vertically so that the combustion products are moving to the mixing volume. The challenge bioaerosol is also fed into the mixing volume, where the inactivation of aerosolized microorganisms occurs. The burner is mounted so that its height can be adjusted. The height

adjustment enables one to change the distance from the flame to the mixing volume and thus tune the temperature and composition of the combustion products interacting with the bioaerosol.

In this study, the main challenge bioaerosol was *B. thuringiensis* serovar kurstaki (Btk), strain SA-1. The culture was obtained in powder from Certis USA Inc. (product # SA-11 SDTC; technical grade concentrate developed for US Army and Air Force). For comparison, *Bacillus atrophaeus* endospores (*B. subtilis* var. *niger* or *B. globigii,* BG) obtained from the US Army Edgewood Chemical Biological Center (Aberdeen Proving Grounds, MD, USA) was also used. Both are well-known surrogate of *B. anthracis*. Bt(k) spores are more preferable as a better stimulant, but the available spore stock needs purification (see below).

The spores were generated from a surfactant-free, de-ionized water suspension using a six-jet Collison nebulizer (BGI Inc., Waltham, MA, USA) operated at 6 L/min. The shear forces inside the nebulizer help de-agglomerate the aerosolized spores. The bioaerosol generation protocol has been validated and utilized in our earlier studies. After exiting the nebulizer's nozzle, the bioaerosol is diluted and charge-equilibrated with a 10-mCi ^{85}Kr charge equilibrator (model 3012, TSI Inc., St. Paul, MN, USA). The system is capable of producing and handling dilution flows from 6 to 120 L/min. In this study, we used a 30 L/min HEPA-filtered dry air flow; this generated a total (diluted) bioaerosol flow of Q = 36 L/min entering the mixing volume horizontally.

After passing the mixing chamber, the aerosol is sampled into three identical cylindrical probes and transported through a 300-mm long cooling system, which reduces the air flow temperature to the room temperature level. In this study, sterile 25-mm filter cassettes (SKC Inc., Eighty Four, PA, USA) equipped with a 25-mm sterile gelatin filter (SKC Inc.) were utilized as bioaerosol collectors demonstrated to be effective for bacterial spores. The collected samples are subjected to culture-based analysis. As a result, an inactivation factor, IF, is determined as the ratio of the culturable spore concentrations obtained without combustion (control) to that after the bioaerosol exposure to the heat and combustion products produced by the flame (exposed).

In the burner, the powder feeder generates a flow by directing a high velocity gas jet on a powder loaded into the threads of a screw. The aerosol jet velocity is controlled by the flow rate of the carrier gas. The mass feed rate of the powder is adjusted independently of the flow rate by changing the thickness of the coating and rate of the screw rotation. The screw is turned by a speed reduction gear train driven by a DC motor. In this system, a stainless steel screw, ¾" (19.05 mm) diameter with 16 threads per inch is used. To prepare the coating, powder is dried and placed in a plastic dish. With the help of a short bristle brush, the powder is deposited into the threads of the screw. The powder in the dish is weighed before and after the screw was coated to determine the loaded powder mass. The screw loaded with powder is enclosed into a cylindrical brass collar and coupled with the motor. The brass collar has feedthroughs for the carrier gas inlet and aerosol outlet. A brass capillary tube ($^1/_{16}$" or 1.59 mm OD) inserted through the carrier gas inlet, was crimped to make a triangular nozzle tip (~0.62 mm on each side) that conforms to the "V" channel of the screw threads. The nozzle tip directs a high velocity nitrogen jet into the thread to efficiently remove and aerosolize the powder. The aerosol

exits through an opposing small diameter brass tube on the feed screw collar (inserted into the aerosol outlet feedthrough). The brass collar together with the aerosol outlet move along the screw during the operation. The aerosol outlet is connected to the burner using flexible plastic tubing.

A typical powder load varied from 0.7 to 1.2 g; it was placed over about 5-cm length of the screw. In preliminary experiments, rates of screw rotation and respective powder feed rates were tested. The range of feed rates selected, 0.5 – 1.14 mg/s, maximized the aerosol flow, while not affecting substantially the flame shape and dimensions. This mode of operation was preferred to minimize the effect of altered temperature and flow profiles on the measurements of the bioaerosol inactivation.

In the burner, acetylene and air are fed through fine brass screens to enhance mixing. The flammable mixture is fed through a tube with a narrowing internal diameter. A thin stainless steel tube placed at the axis of the burner is used to inject the particles carried by nitrogen. The produced flame is laminar.

The temperature in the mixing volume was measured by thermocouples (Omega Engineering, type E, part # TJ36-CAXL-116E-6) and registered by a 2-channel thermometer (HH66U, Omega Engineering). Six thermocouples at a time were inserted through a set of drilled orifices into the stainless pipes with brass tubing feedthroughs, and moved to the positions indicated in the central cross-section. The thermocouples enabled quantification of the air temperature patterns in the mixing volume under different experimental conditions (including the flame characteristics and proximity of the burner to the mixing chamber). However, the results achieved using this protocol should be treated carefully considering that (a) the thermocouples disturb the flow and affect the measured temperature through thermal conductivity, (b) the best-achievable linear increment of 5 mm may not be sufficient to resolve the spatial variability in the chamber temperature (especially given a 1-mm precision limit of the linear measurement with a ruler), and (c) the measurement cannot capture the short-term variations in the local flow velocity and temperature. The preliminary testing of the temperature measurement protocol showed that the effect of powder added to the flame is smaller and, thus, is undetectable compared to the thermal variability observed during normal burner operation.

To further advance the experimental capability for investigating the effect of heat and chemical stresses on the survival of aerosolized spores, the above facility was enhanced. Existing protocols for the evaluation of biocidal materials do not differentiate between the viability losses caused by heat stress and by combustion products. In this study, a two-configuration experimental approach was developed to address the situations when the bioaerosols is supplied: (i) through the combustion zone so that the microorganisms are exposed to both the thermal and chemical inactivation and (ii) downstream from the combustion zone where the air temperature substantially decreases so that the viability loss occurs primarily due to exposure to combustion products. Two experimental setups were designed and built to implement these configurations. A hydrocarbon fuel flame seeded with three fuel additives, which were delivered to the burner from a powder disperser, represented the tested combustion environments. One of the powders contained aluminum with embedded iodine that was designed to be released at the aluminum melting temperature. In experiments performed with both setups, *Bacillus* endospores

were exposed to the combustion environments, and the spore inactivation was quantitatively characterized for each set of conditions using a culturable enumeration of the exposed and non-exposed bioaerosol samples. Additionally, the first configuration was utilized for the tests, in which the burner was replaced with an axial heater providing specific temperature conditions for the challenge bioaerosol with no release of combustion products. It was determined that inactivation levels associated with the heat and chemical stresses may be comparable. Consequently, the heat and chemical factors may produce a synergistic effect.

To evaluate the influence of various factors (including the exposure time) on the spore inactivation, additional modifications were performed for the experimental set-up. The flow-through exposure chamber was extended by adding five steel sections downstream (Fig. 2.1.2). Additionally, the radial electrical heaters were installed to maintain a constant air flow temperature longitudinally within a selected distance from the initial point. Each heater (H_1 through H_8) was powered by a separate electrical regulator, which allowed for a precise power adjustment across the exposure distance. To control and manage the temperature profile, movable thermocouples were installed at different positions. Each thermocouple measured the air temperature at three points: at the center, half-radius, and radius (pre-wall) of a selected cross-section so that the cross-sectional and longitudinal temperature distributions were obtained in the exposure chamber. The set-up enabled us to achieve – by varying the heaters' power – a uniform air flow temperature profile along a specific distance for a specific temperature level, burner position, and flow rate through the exposure chamber. In a majority of our experiments conducted this year, we targeted the temperature level of 200°C – high enough to maintain the iodine released during a tested FNM combustion in the gaseous phase and, at the same time, low enough to make the heat-induced spore inactivation negligible compared to the chemical one. To achieve a desirable exposure time at that temperature, the voltage was applied to a specific set of heaters, e.g., only H_8, or H_6 through H_8, or H_4 through H_8, etc. (others, downstream of the chosen point were turned off). It was observed that once the flow passes the last operating heater, the air temperature decreased from 200°C to 155°C within a distance as short as ~20 mm. At that decreased temperature, essentially no iodine remains in the gaseous phase so that the spore exposure to the iodinated component can be considered to be limited to the zone L_H where the heaters are on. In the first approximation, the average air flow velocity was calculated as the ratio of the flow rate through the chamber to the cross-sectional area; the exposure time was calculated as L_H divided to the average air velocity.

The modified set-up allowed establishing a uniform temperature profile (both cross-sectionally and longitudinaly). An example is presented in Table 2.1.1. By using various combinations of heaters and through managing the total flow rate, we were able to conduct the inactivation testing at exposure times ranging from ~0.1 to ~2.01 s.

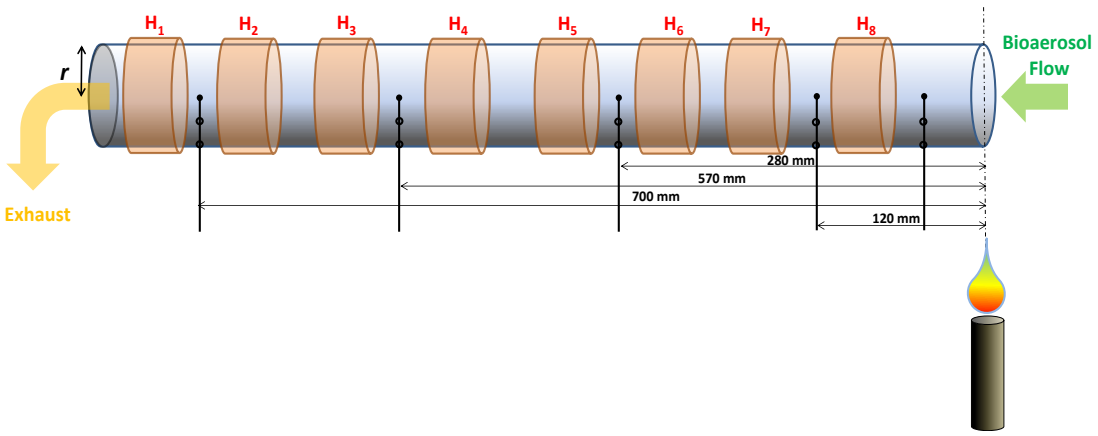

Fig. 2.1.2. Modification of the experimental set-up (exposure chamber with heaters).

Table 2.1.1. Air temperatures measured for the longest time of exposure (2.01 s)

Cross-sectional coordinate	*Longitudinal coordinate, mm*				
	50	*120*	*280*	*570*	*700*
0	**216**	**210**	**205**	**200**	**198**
r/2	**208**	**210**	**205**	**205**	**205**
r	**205**	**216**	**210**	**210**	**215**

By moving the burner vertically up and down, we were able to establish different air temperature conditions in the exposure chamber. Two vertical positions were selected for the burner: (1) a lower one, L = 325 mm, to establish a relatively low exposure temperature level (at which the heat-induced stress is negligibly small and the inactivation takes place primarily due to the chemical interaction) and (2) a higher one, L = 415 mm (at which the inactivation occurs due to both the heat and the chemical effect).

2.2. **Development of purification protocol for Bt(k)**

Depending on the source, commercially available Btk spores may be mixed with flow enhancer and tracer materials (e.g., Technical Grade Javelin from the US Air Force, FL). Those were not chosen. The chosen Btk (from Certis USA Inc.) contained not only spores but protein crystals. Given that Btk serves in this study as a simulant of *B. anthracis* that does not come with the crystals, we decided to use a purified Btk suspension. The purification protocol was adopted from Dr. Charles Neely and modified. Briefly, Bt(k) spores were suspended in 50% ethanol (pH 9.0) and washed by centrifugation at 6000 rpm for 25 minute. The supernatant was discarded and the process was repeated 2-3 times until the supernatant was clear. Then the spores were resuspended in cold acetone and stored in freezer overnight. The acetone-spore suspension was filtered to complete dryness and the dry powder was crushed in mortar pestle. The powder

was sieved using a metal screen and stored for later sue. As a result, we managed to change the crystal-to-spore ratio from 1.8 (initial suspension, Fig. 2.2.1 left) to 0.02 (Fig. 2.2.1 right).

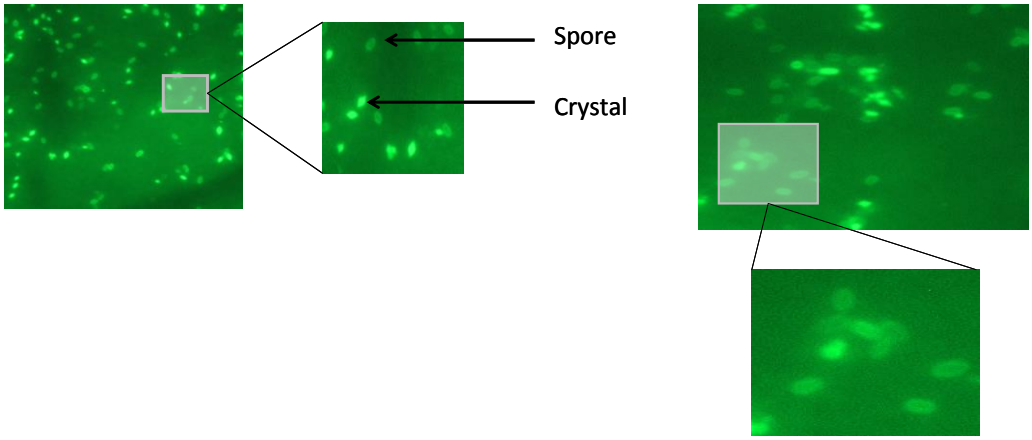

Figure 2.2.1. Purification of Btk (removing crystals).

2.3. Inactivation of *Bacillus* spores at a fixed exposure time (0.33 s) and two positions of the burner: comparison of different combustion materials for BG and Bt(k)

While Bt(k) was considered the main challenge aerosol simulating *B. anthracis* in this study, the first set of tests aiming at quantifying the inactivation factor of new materials was performed with BG spores. The reason is that BG spores have been historically widely used in the DoD community and it was our intention to generate the material performance data with this "older" Ba surrogate to link the present and the past research efforts on the spore inactivation.

The BG spore inactivation data are presented in Fig. 2.3.1A for the two selected vertical positions of the burner and four combustion sources, including unseeded air-acetylene flame as well as the flame seeded with Al (3-4.5 μm), $Al{\cdot}I_2$, and $Al{\cdot}B{\cdot}I_2$ powders (the latter had a weight ratio of 69:11:20). Unlike our earlier measurements (Grinshpun et al., 2012), where the bioaerosol was co-flowing with the combustion products of a seeded air-acetylene flame and exposed to higher temperatures and higher temperature gradient flow fields, adding Al powder did not enhance the spore inactivation as compared to a powder-free flame.

No significant loss of viability was caused by either unseeded or Al-seeded flames when the burner was at its low position. This suggests that the thermal effect is insufficient, and that the cooled off and condensed combustion products of Al do not inactivate. With the burner at the high position, about 90% of spores were inactivated (IF~10) by both the unseeded flame and by the flame with Al powder. This is consistent with earlier results (Grinshpun et al., 2010), suggesting the achieved temperature level produced heat stress sufficient to inactivate approximately 90% of spores.

Both iodine-containing materials exhibited IF-values higher than Al by an order of magnitude at the low burner position and two to three orders of magnitude at the high position.

For the lower position, only a small fraction of the released iodine remained in the gaseous phase in the exposure chamber, thus allowing for IF of about 10 (Fig. 2.3.1A). When the burner was moved higher, the iodinated powders produced much greater IFs: geometric means = 733 for Al·I_2 and 2,654 for Al·B·I_2 (weight ratio = 69:11:20); the difference between the composites was significant (t-test: $p<0.05$). The major share of this inactivation is believed to be associated with the chemical effect because the thermal effect under this condition can only produce IF of ~10. Interestingly, the enhanced effect of Al·B·I_2 occurred despite the overall lower iodine concentration in this material compared Al·I_2 and also in spite of somewhat lower combustion temperatures (see Section 1 above). This effect highlights the importance of slow release of iodine in the combustion products for inactivation of aerosolized spores.

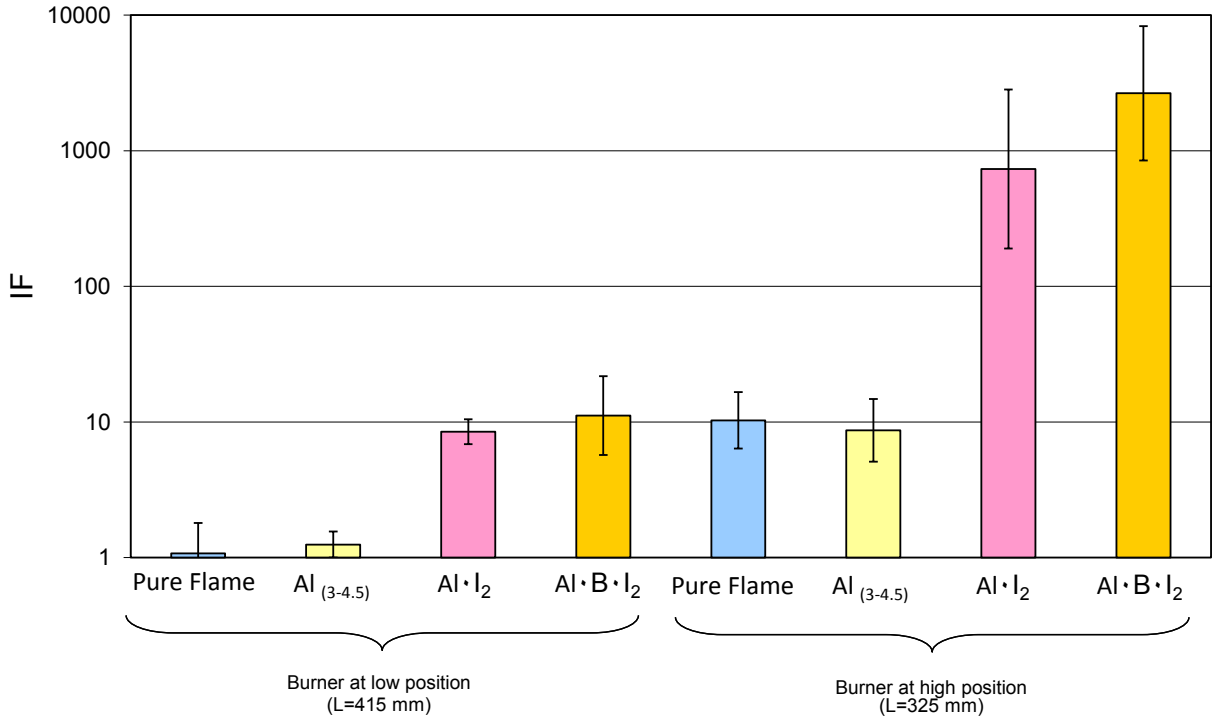

Figure 2.3.1A. Inactivation of aerosolized BG spores with different materials under different exposure conditions. Exposure time is estimated to be 0.33 s. Each color bar represents the geometric mean value with the error bars representing the geometric standard deviation calculated from 9 to 18 measurements.

Similar experiments were conducted with Bt(k) spores. The results are presented in Fig. 2.3.1B below. While some difference in IF's geometric mean values obtained with BG and Bt(k) spores are seen, both species demonstrate similar responses to the exposures tested. Generally, Bt(k) shows slightly higher resistance to chemical stress compared to BG (which was expected).

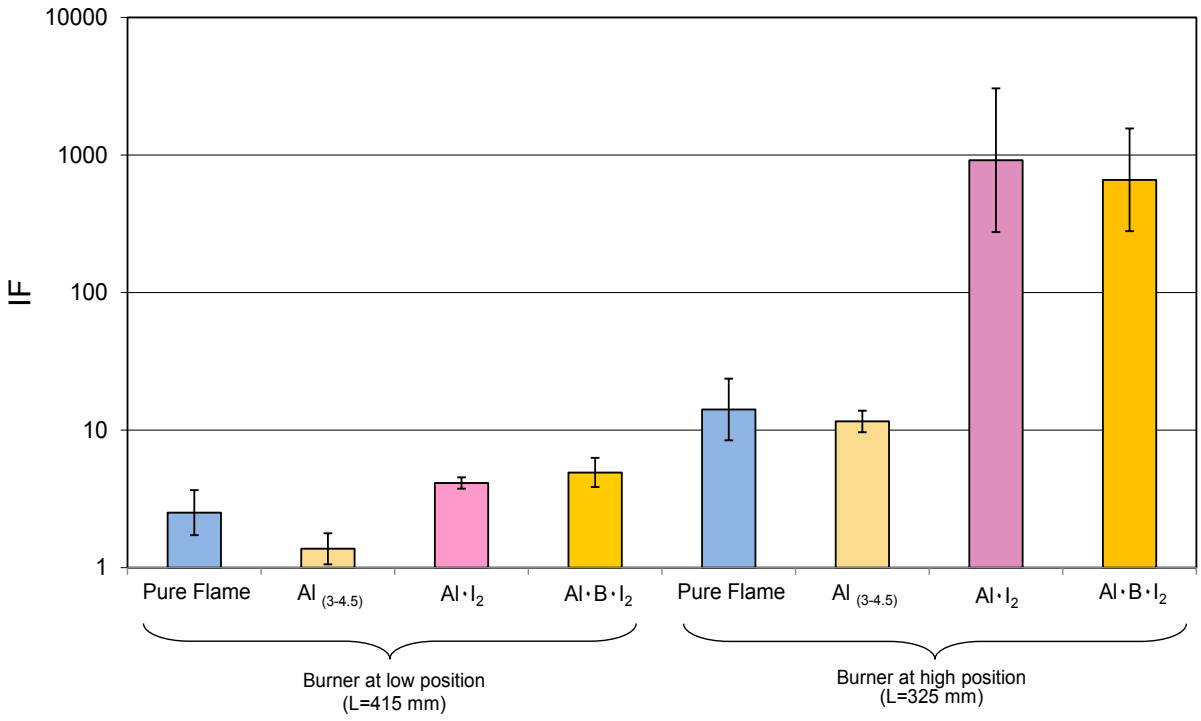

Figure 2.3.1B. Inactivation of aerosolized Bt(k) spores with different materials under different exposure conditions. Exposure time is estimated to be 0.33 s. Each color bar represents the geometric mean value with the error bars representing the geometric standard deviation calculated from 15 to 21 measurements.

2.4. Targeted testing of aluminum and boron containing materials with Bt(k). Summary of the biocidal performance at a fixed exposure time (0.33 s)

Figure 2.4.1 summarizes the results on the Bt(k) spore inactivation obtained for various combustion materials tested in this project at two position of the burner. It is remarkable that Al+B containing formulations produced the highest IF values. Interestingly, the enhanced effect of Al·B·I_2 occurred despite the overall lower iodine concentration in this material compared Al·I_2 and also in spite of somewhat lower combustion temperatures. This effect highlights the importance of slow release of iodine in the combustion products for inactivation of aerosolized spores. On the other hand, for Al·B·I_2, the weight ratio (specifically, the boron component of Al·B·I_2) was shown to affect the inactivation (IF for the formulation containing 20% of boron was an order of magnitude higher than the one containing 11%).

We anticipate that kinetics of iodine release is qualitatively different in the materials with higher boron concentration. A slower, more gradual release of iodine from boron (which burns slower than aluminum) may enhance the mixing of iodine-bearing gas species with the challenge bioaerosol. It is possible that boron combustion products have biocidal effects of their own. It is also possible that aside from I_2 and HI, expected to be produced, new, more biocidal boron and

iodine-bearing gas species are generated when burning materials with higher boron concentrations. Thermodynamics of the respected phases is not well known; additional work is needed to identify the specific products generated and to establish their relative biocidal properties.

2.5. **Inactivation of Bt(k) spores by materials: $Al{\cdot}CHI_3$ and $Al{\cdot}NbCl_5$**

Additionally, the spore inactivation was investigated with two other materials: $Al{\cdot}CHI_3$ and $Al{\cdot}NbCl_5$. The same exposure time (≈0.33 s) was used. The results collected suggest that the $Al{\cdot}CHI_3$ powder had a measurable, but limited potency to inactivate the aerosolized Bacillus spores. Even when the temperature in the exposure zone was increased by moving the burner to the high position (L = 415 mm), the $Al{\cdot}CHI_3$-seeded flame generated IF values substantially below 100 (geometric mean = 27.0) while a pure powder-free flame produced IF=10.3 and $Al{\cdot}I_2$ produced IF of about 1,000 under the same conditions. While this result is presently not well interpreted, the finding appears to be important for future development of reactive materials with biocidal combustion products. One possible explanation may be associated with a lower effectiveness of chloride-bearing species compared to their iodine counterparts. The newly-developed Al-$NbCl_5$ was found to produce rather high inactivation effect against Bt(k).

2.6. **Effect of exposure time on inactivation of BG and Bt(k) spores**

To study the kinetics of the spore inactivation process, experiments with BG and Bt(k) were performed at various times of exposure (τ ~0.12 to ~2.01 s) and the lower position of the burner. Figure 2.6.1 presents the relationships between IF and the time of exposure for Bt(k) and BG spores exposed to the combustion products of $Al{\cdot}I_2$ and $Al{\cdot}B{\cdot}I_2$ at a narrow range of air temperatures, 198–216°C. All tests were performed at the low position of the burner. It is seen that IF is exponentially dependent on the exposure time for both species and FNMs (almost perfectly following the Arrhenius formula). Furthermore, within the microorganism species (either Bt(k) or BG) no statistically significant difference was found between the relationships determined at the two different composites ($p>0.05$).

The data presented in Fig. 2.6.1 can be treated as initial quantitative kinetic information characterizing inactivation rates of bioaerosol particles exposed to combustion products of halogen-containing reactive materials. Once similar data are available for a range of temperatures and for a set of iodine concentrations, a comprehensive model compatible with the present hydrodynamic codes describing explosives can be developed. The model will enable one to predict the bioaerosol inactivation rate in a blast produced by an explosive charge containing FNM developed in this program.

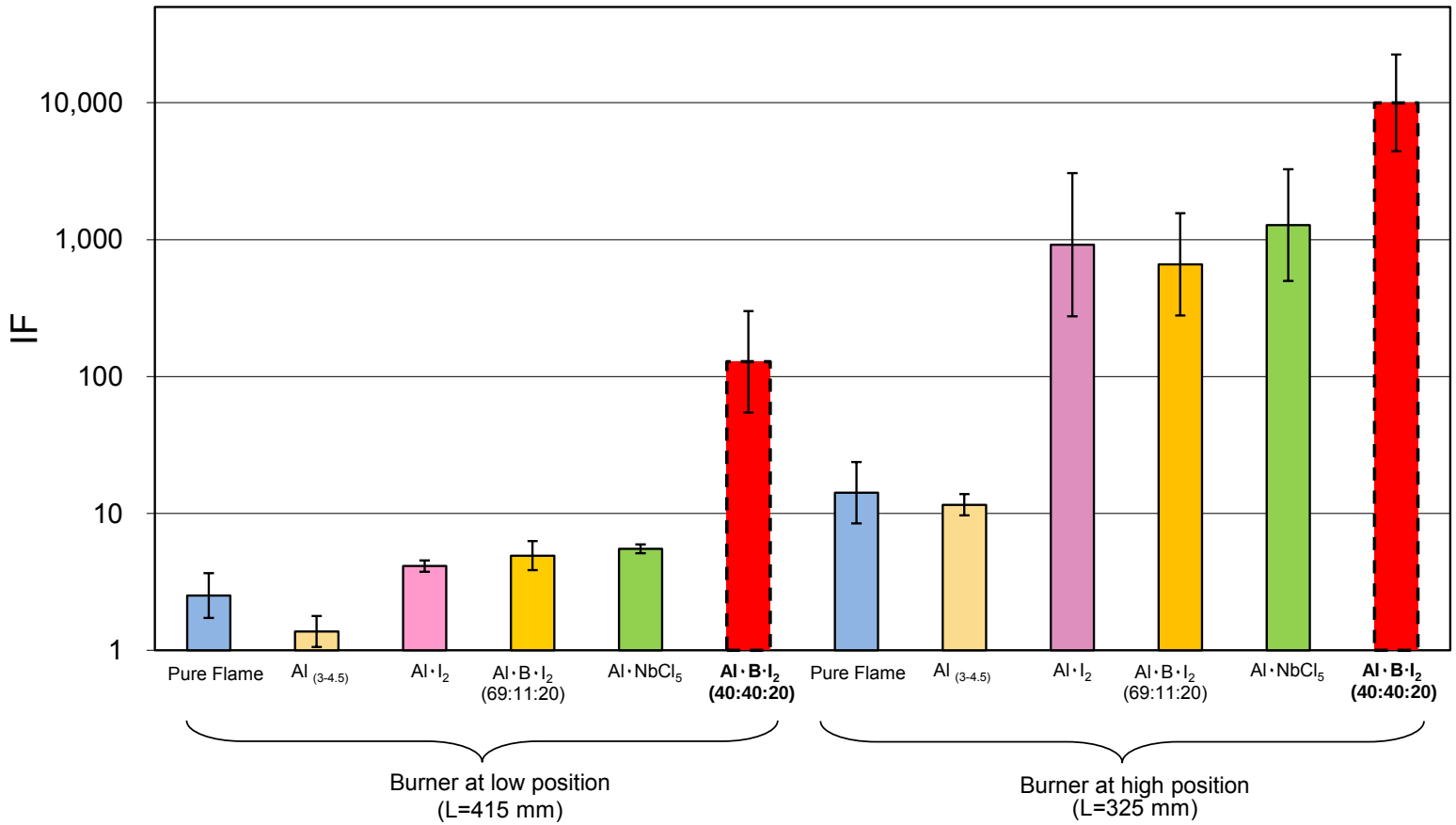

Figure 2.4.1. Inactivation of aerosolized Bt(k) spores with different materials under different exposure conditions. Exposure time is estimated to be 0.33 s. Each color bar represents the geometric mean value with the error bars representing the geometric standard deviation calculated from 15 to 21 measurements.

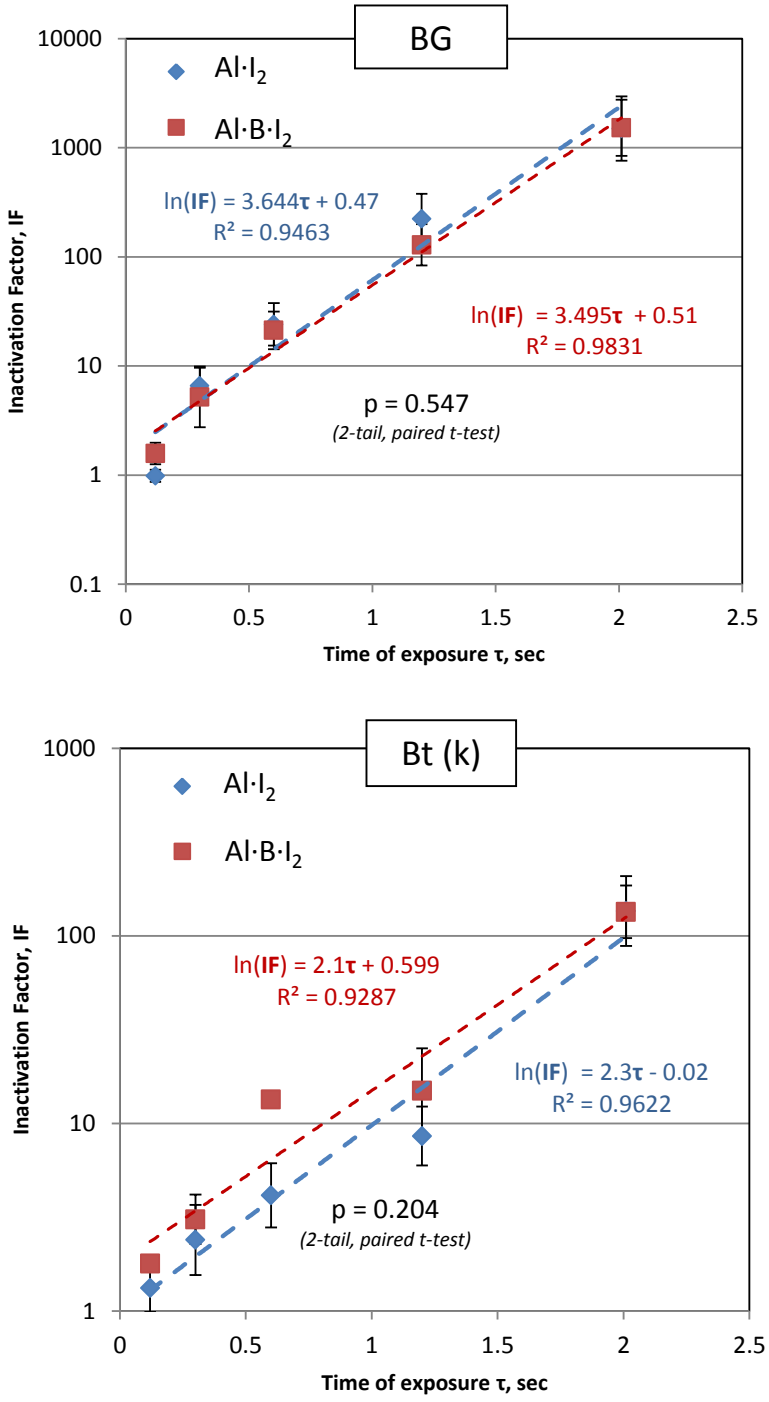

Figure 2.6.1. Inactivation of aerosolized spores of BG and Bt(k) as a function of time.

2.7. **Culturability of *Bacillus* spores on aerosol collection filters exposed to airborne combustion products of Al, Mg, and B·Ti**

A bioaerosol sample (often collected on a filter for further culture-based analysis) also contains combustion products, which may influence the microbial culturability and, thus, impact the outcome. We have examined the interaction between spores deposited on collection filters using BG and Bt(k) and incoming combustion products of Al as well as Mg and B·Ti. Spores extracted from Teflon, polycarbonate, mixed cellulose ester (MCE), and gelatin filters (most common filter media for bioaerosol sampling), which were exposed to combustion products during a short-term sampling, were analyzed by cultivation. Surprisingly, we observed that aluminum combustion products enhanced the culturability of Bt (but not BG) spores on Teflon filters increasing the culturable count by more than an order of magnitude. Testing polycarbonate and MCE filter materials also revealed a moderate increase of culturability although gelatin did not. No effect was observed with either of the two species interacting on either filter media with products originated by combustion of Mg and B·Ti. Figures 2.7.1 and 2.7.2 summarize the findings. Survival ratio on the y-axis presented in these figures is 1/IF. Sample contamination, spore agglomerations, effect of a filter material on the spore survival, changes in the spore wall ultrastructure and germination, as well as other factors were explored to interpret the findings. The study raises a question about utilization of certain filter materials for collecting airborne bio-threat agents in combustion environments.

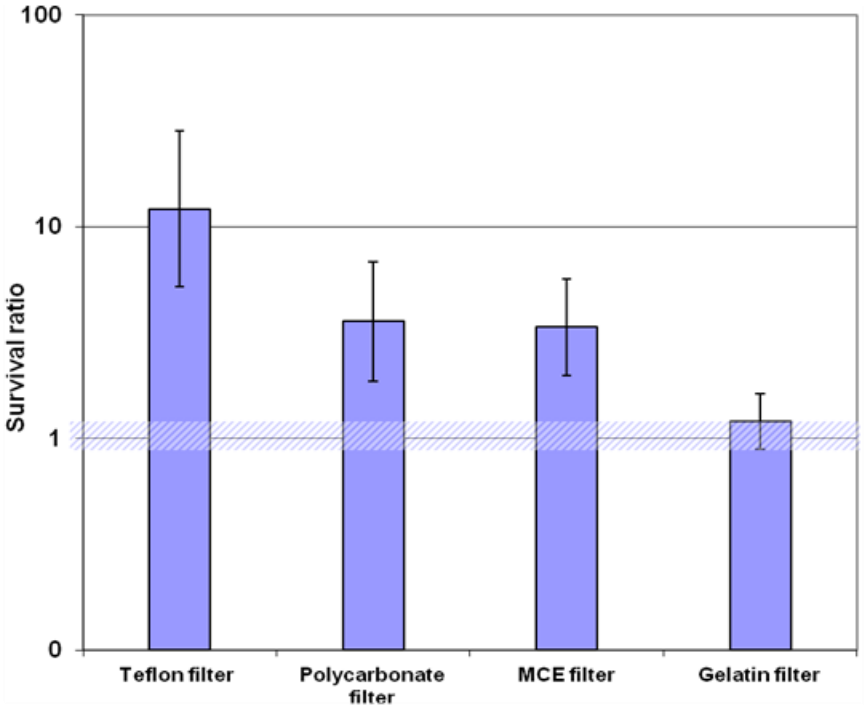

Figure 2.7.1. Survival ratio of Bt(k) spores (purified) on four filter media exposed to incoming Al combustion products for 1 min (each bar represent a geometric mean of 10 replicate measurements, the error bars represent geometric standard deviation).

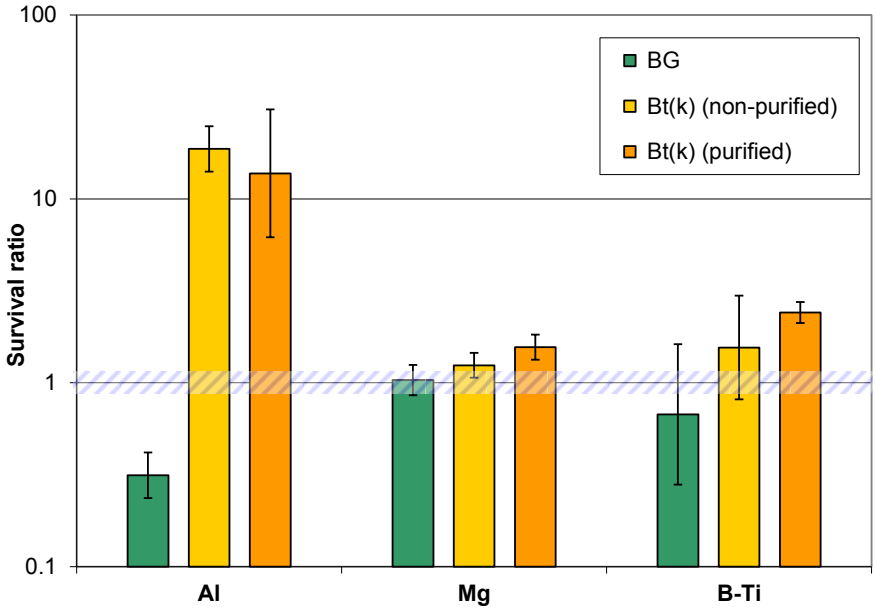

Figure 2.7.2. Survival ratio for Bt(k) spores (with and without crystals) and BG spores on Teflon filter media when exposed to incoming combustion products of Al, Mg, and B-Ti for 1 min (each bar represent a geometric mean of at least 10 replicate measurements, the error bars represent geometric standard deviation).

REFERENCES

A. Abraham; S. Zhang; Y. Aly; M. Schoenitz; E. L. Dreizin, Advanced Engineering Materials (2014)

J. P. Agrawal, Propellants, Explosives, Pyrotechnics 30 (5) (2005) 316-328

Y. Aly; S. Zhang; M. Schoenitz; V. K. Hoffmann; E. L. Dreizin; M. Yermakov; R. Indugula; S. A. Grinshpun, Combustion and Flame 161 (1) (2014) 303-310.

A. F. Armington; G. F. Dillon; R. F. Mitchell; A. F. C. R. L. L. G. H. F. MASS.; A. F. C. R. Laboratories, The Preparation of High-purity Boron Via the Iodide, Defense Technical Information Center, 1964, p.^pp.

A. Azhagurajan; N. Selvakumar; M. Mohammed Yasin, Process Safety Progress 31 (1) (2012) 19- 23

D. M. Badgujar; M. B. Talawar; S. N. Asthana; P. P. Mahulikar, Journal of Hazardous Materials 151 (2-3) (2008) 289-305.

D. M. Bieliński; L. Ślusarski; P. Głąb, Journal of Applied Polymer Science 105 (1) (2007) 177-189

C. J. Bulian; J. A. Puszynski; J. J. Swiatkiewicz in: Tunability of nanoenergetic materials, 2008; 2008.

M. W. Chase, J. Phys. Chem. Ref. Data, Monograph 9 (1998) 1-1951.

R.-H. Chen; C. Suryanarayana; M. Chaos, Adv. Eng. Mater. 8 (Copyright (C) 2012 American Chemical Society (ACS). All Rights Reserved.) (2006) 563-567 10.1002/adem.200600002.

K. O. Christe; R. Haiges; W. W. Wilson, Halchem V, Sardinia (2010)

K. O. Christe; R. Haiges in: Iodine fluoride, oxofluoride and oxide chemistry, 2013; American Chemical Society: 2013; pp FLUO-22.

Z. Doorenbos; J. Puszynski; D. Kapoor in: The effect of particle morphology on the combustion properties of MIC materials, 2009; 2009.

E. L. Dreizin; M. Schoenitz, Nano-composite Energetic Powders Prepared by Arrested Reactive Milling (2009).

E. L. Dreizin; C. Badiola; S. Zhang; Y. Aly, International Journal of Energetic Materials and Chemical Propulsion 10 (4) (2011) 22.

B. Z. Eapen; V. K. Hoffmann; M. Schoenitz; E. L. Dreizin, Combustion Science and Technology 176 (7) (2004) 1055-1069 10.1080/00102200490426433.

O. C. Eneh, Research Journal of Environmental Toxicology 6 (3) (2012) 65-87

A. Ermoline; E. L. Dreizin, Chemical Physics Letters 505 (1-3) (2011) 47-50 10.1016/j.cplett.2011.02.022.

C. Farley; M. Pantoya, Journal of Thermal Analysis and Calorimetry 102 (2) (2010) 609-613 10.1007/s10973-010-0915-5.

L. J. Gillespie; L. H. D. Fraser, Journal of the American Chemical Society 58 (11) (1936) 2260-2263

S. A. Grinshpun; C. Li; A. Adhikari; M. Yermakov; T. Reponen; M. Schoenitz; E. Dreizin; V. Hoffmann; M. Trunov, Aerosol and Air Quality Research 10 (5) (2010) 414-424 10.4209/aaqr.2010.04.0041.

S. A. Grinshpun; A. Adhikari; M. Yermakov; T. Reponen; E. Dreizin; M. Schoenitz; V. Hoffmann; S. Zhang, Environmental Science and Technology 46 (13) (2012) 7334-7341 10.1021/es300537f.

S. A. Grinshpun; A. Adhikari; M. Yermakov; T. Reponen; E. Dreizin; M. Schoenitz; V. Hoffmann in: Neutralization of Viable Aerosolized Microorganisms due to Exposure to Combustion of Reactive Materials, European Aerosol Conference, Granada, Spain, 2012; Granada, Spain, 2012a; pp #A-WG02S1P19.

C. E. Johnson; K. T. Higa, MRS Online Proc. Libr. 1521 (Copyright (C) 2013 American Chemical Society (ACS). All Rights Reserved.) (2013) 2013.46/1-2013/46/6 10.1557/opl.2013.46.

G. Jian; S. Chowdhury; J. Feng; M. R. Zachariah, 2012 AIChE Annual Meeting (2012) 388n.

M. A. Korchagin; B. B. Bokhonov, Combustion, Explosion and Shock Waves 46 (2) (2010) 170-177 10.1007/s10573-010-0026-4.

B. J. McBride; S. Gordon, in: NASA RP 1311, 1996.

B. S. Murty; S. Ranganathan, International Materials Reviews 43 (3) (1998) 101-141

R. W. Nelson, Physics Today 56 (11) (2003) 32-37.

A. S. Rogachev; A. S. Mukasyan, Combustion, Explosion and Shock Waves 46 (3) (2010) 243-266 10.1007/s10573-010-0036-2.

P. R. Santhanam; V. K. Hoffmann; M. A. Trunov; E. L. Dreizin, Combustion Science and Technology 182 (7) (2010) 904-921 10.1080/00102200903418278.

M. Schoenitz; E. L. Dreizin, Journal of Materials Research 18 (8) (2003) 1827-1836

M. Schoenitz; E. Dreizin, Journal of Propulsion and Power 20 (6) (2004) 1064-1068

H. Shemer; N. Narkis, Ultrasonics Sonochemistry 12 (6) (2005) 495-499

Y. L. Shoshin; E. L. Dreizin, Combustion and Flame 145 (4) (2006) 714-722 10.1016/j.combustflame.2005.11.006.

Y. L. Shoshin; M. A. Trunov; X. Zhu; M. Schoenitz; E. L. Dreizin, Combustion and Flame 144 (4) (2006) 688-697 10.1016/j.combustflame.2005.08.037.

D. Stamatis; Z. Jiang; V. K. Hoffmann; M. Schoenitz; E. L. Dreizin, Combustion Science and Technology 181 (1) (2009) 97-116 10.1080/00102200802363294.

M. J. Starink, Thermochimica Acta 404 (1-2) (2003) 163-176

A. N. Sterletskii; A. Y. Dolgoborodov; I. V. Kolbanev; M. N. Makhov; S. F. Lomaeva; A. B. Borunova; V. E. Fortov, Colloid Journal 71 (6) (2009) 852-860 10.1134/s1061933x09060155.

K. T. Sullivan; N. W. Piekiel; S. Chowdhury; C. Wu; M. R. Zachariah; C. E. Johnson, Combustion Science and Technology 183 (3) (2011) 285-302

K. T. Sullivan; C. Wu; N. W. Piekiel; K. Gaskell; M. R. Zachariah, Combustion and Flame 160 (2) (2013) 438-446 10.1016/j.combustflame.2012.09.011.

C. Suryanarayana, Progress in Materials Science 46 (1-2) (2001) 1-184 10.1016/s0079-6425(99)00010-9.

S. M. Umbrajkar; S. Seshadri; M. Schoenitz; V. K. Hoffmann; E. L. Dreizin, Journal of Propulsion and Power 24 (2) (2008) 192-198 10.2514/1.31762.

T. S. Ward; M. A. Trunov; M. Schoenitz; E. L. Dreizin, International Journal of Heat and Mass Transfer 49 (25-26) (2006) 4943-4954 10.1016/j.ijheatmasstransfer.2006.05.025.

E. Wiberg; N. Wiberg; A. F. Holleman, Inorganic chemistry, San Diego, Calif. : Berlin: Academic Press, W. de Gruyter, 2001, p.^pp. 930.

S. Zhang; M. Schoenitz; E. L. Dreizin, Journal of Physical Chemistry C 114 (46) (2010a) 19653-19659 10.1021/jp108171k.

S. Zhang; M. Schoenitz; E. L. Dreizin, Journal of Physics and Chemistry of Solids 71 (9) (2010b) 1213-1220 10.1016/j.jpcs.2010.04.018.

S. Zhang; C. Badiola; M. Schoenitz; E. L. Dreizin, Combustion and Flame 159 (5) (2012) 1980-1986 http://dx.doi.org/10.1016/j.combustflame.2012.01.004.

S. Zhang; M. Schoenitz; E. L. Dreizin, International Journal of Energetic Materials and Chemical Propulsion 11 (4) (2012a) 353-373

What opportunities for training and professional development has the project provided?

The primary mission of this effort is research. However, the grant has provided useful opportunities for training and professional development. Five faculty members (including one junior Assistant Professor), a postdoctoral fellow, two research fellows and three graduate students from UC and NJIT have been involved in this grant. Some fragments of this study were included in the graduate courses taught by the PI and Co-PI in their respective institutions.

Additionally, the grant provided the travel support to team members to attend national and international scientific conferences and other professional meetings, including SHS 2013, XII International Symposium On Self-Propagating High Temperature Synthesis (October 2013), AIChE Annual Meetings (2011-2015), as well as American and international aerosol conferences (2011-2015). The above allowed for a productive interaction of the project team members with other scientists and contributed to the investigators' professional development helping to advance their research, teaching and mentoring efforts.

How have the results been disseminated to communities of interest?

The data collected during the grant performance period were disseminated to the professional community through collaborative efforts initiated by Dr. Su Peiris of DTRA that involved other DTRA/DoD-supported research programs from Loyola University (Chicago), the Penn State University, University of Connecticut, University of Maryland, Naval Surface Warfare Center at Indian Head, and others.

The results of this study were presented at four Technical Review meetings held by DTRA annually. Extensive discussions with other DTRA grantees that took place at these meetings produce a considerable positive impact on the project and helped develop fruitful collaborations with several researchers nationwide.

Directly resulting from this DTRA-sponsored effort, 5 papers were published, 1 submitted, and three are in preparation for publication in major peer-reviewed journals. In addition, 16 presentations at national and international conference have been given. See below the list of published and submitted journal papers and conference presentations.

PUBLICATIONS IN PEER-REVIEWED JOURNALS (in chronological order)

Grinshpun, S.A., Adhikari, A., Yermakov, M., Reponen, T., Dreizin, E., Schoenitz, M., Hoffmann, V., and Zhang, S. (2012) Inactivation of Aerosolized BG Endospores and MS2 Viruses by Combustion of Reactive Materials. *Environmental Science and Technology*, 46:7334-7341.

Zhang, S., Schoenitz, M., and Dreizin, E.L. (2013) Nano-structured Aluminum Powders with Modified Protective Surface Layers, *Material Research Society Symposium Proceedings*, 1521:1-6, DOI 10.1557/opl.2013.130.

Aly, Y., Zhang, S., Schoenitz, M., Hoffmann, V., Dreizin, E.L., Yermakov, M., Indugula, R., and Grinshpun, S.A. (2014) Iodine-Containing Aluminum-Based Fuels for Inactivation of Bioaerosols *Combustion and Flame*, 161:303-310.

Abraham, A., Zhang, S., Aly, Y, Schoenitz, M, and Dreizin, E.L. (2014) Aluminum-iodoform Composite Reactive Material. *Advanced Engineering Materials*, 16(7):909-917

Abraham, A., Obamedo, J., Schoenitz, M., and Dreizin, E.L. (2015) Effect of Composition on Properties of Reactive Al·B·I2 Powders Prepared by Mechanical Milling. J*ournal of Physics and Chemistry of Solids*, 83: 1-7.

Adhikari, A., Yermakov, M., Indugula, R., Reponen, T., Driks, A., and Grinshpun, S.A. (2015) Culturability of Bacillus Spores on Aerosol Collection Filters Exposed to Airborne Combustion Products of Al, Mg, and B·Ti. *Biotechnology and Bioengineering* (submitted).

PRESENTATIONS (in chronological order)

Grinshpun, S.A., Yermakov, M., Adhikari, A., Reponen, T., Zhang, S., Hoffmann, V., Schoenitz, M., and Dreizin, E. (2011) How Combustion of Energetic Materials Affects Viability of Aerosolized Bio-agents, *Abstracts of the 7th Asian Aerosol Conference* (Xi'an, People's Republic of China, August 17-19, 2011), #ID13(IIIh).

Grinshpun, S.A., Adhikari, A., Yermakov, M., Reponen, T., Dreizin, E., Schoenitz, M., and Hoffmann, V. (2011) Investigation of Inactivation of Aerosolized Microorganisms in Combustion Environments: a Two-configurational Experimental Approach, *Abstracts of the 30th Annual Conference of the American Association for Aerosol Research* (Orlando, Florida, U.S.A., October 3-7, 2011), #1D.7.

Grinshpun, S.A., Adhikari, A., Yermakov, M., Reponen, T., Dreizin, E., Schoenitz, M., and Hoffmann, V. (2012) Neutralization of Viable Aerosolized Microorganisms due to Exposure to Combustion of Reactive Materials, *Abstracts of the European Aerosol Conference* (Granada, Spain, September 2-7, 2012), #A-WG02S1P19.

Grinshpun, S.A., Yermakov, M., Indugula, R., Adhikari, A., and Reponen, T. (2012) Collection of Aerosolized Bacterial Endospores from Post-Explosion/Combustion Air Environments, *Abstracts of the 31st Annual Conference of the American Association for Aerosol Research* (Minneapolis, Minnesota, U.S.A., October 8-12, 2012), #4CH.4.

Dreizin, E.L. (2013) Metal Based Reactive Nanocomposites Prepared by Cryomilling. Seminar, Beijing Institute of Technology, Beijing, China (invited speaker)

Zhang, S. and Dreizin E.L. (2012) Nano-Structured Aluminum Powders with Modified Protective Surface Layers *AIChE Annual Meeting* (Pittsburgh, PA, U.S.A., November 1, 2012).

Nie H., Zhang S., Schoenitz, M., and Dreizin, E.L. (2012) Effect of Particle Size on the Reaction of Aluminum Powders with Water. *MRS Fall Meeting*, Session OO1: Thermite and Oxidation Reactions: Properties and Processing I (Boston, MA, U.S.A., November 26, 2012).

Grinshpun, S.A., Yermakov, M., Indugula, R., He, K., Reponen, T., Dreizin, E., Schoenitz, M., Zhang, S., Aly, Y. (2013) Inactivation of Aerosolized Spores in Combustion Environments Using Filled Nanocomposite Materials: Study with Two Surrogates of Bacillus Anthracis, *Abstracts of the European Aerosol Conference* (Prague, Czech Republic, September 1-6, 2013).

Grinshpun, S.A., Yermakov, M., Indugula, R., He, K., Reponen, T., Dreizin, E., Schoenitz, M., Zhang, S., Aly, Y. (2013) Survival of Aerosolized Simulants of Bacillus Anthracis Exposed to Combustion Products of Novel Halogen-Containing Reactive Materials, *Abstracts of the 32nd Annual Conference of the American Association for Aerosol Research* (Portland, Oregon, U.S.A., September 30 – October 4, 2013), #10BA.6.

Abraham, A., Schoenitz, M., and Dreizin, E.L. (2013) Metal-based Reactive Materials. *AIChE Annual Meeting* (San Francisco, U.S.A., November 3-8, 2013).

Abraham, A., Schoenitz, M., and Dreizin, E.L. (2013) Metal-based Reactive Materials with Biocidal Reaction Products. *XII International Symposium on Self-Propagating High Temperature Synthes*is (South Padre Island, TX, U.S.A., October 21 – 24, 2013).

Grinshpun, S.A. (2014) Inactivation of Viable Bioaerosol Particles: from Indoor Air Quality to Bio-defense Applications [Keynote], *Abstracts of the International Aerosol Conference* (Busan, South Korea, August 28 – September 2, 2014), PO69-1.

Grinshpun, S.A., Yermakov, M., Indugula, R., Adhikari, A., Reponen, T., Dreizin, E., and Schoenitz, M. (2014) Exposure of Aerosolized Bacillus Spores to Combustion Products of Novel Reactive Biocidal Materials: Kinetics of Inactivation Process. *Abstracts of the 33nd Annual Conference of the American Association for Aerosol Research* (Orlando, Florida, U.S.A., October 20-24, 2014), #13BA.1.

Grinshpun, S.A., Yermakov, M., Indugula, R., Reponen, T., and Weber, A.W. (2015) Evaluation of Personal Inhalable Aerosol Samplers with Different Filters for Collecting Surrogates of Bacillus Anthracis, *Abstracts of the European Aerosol Conference* (Milan, Italy, September 6-11, 2015), 1IEH_P006.

Grinshpun, S.A., Yermakov, M., Indugula, R., Elmashae, Y., Reponen, T., and Weber, A.W. (2015) Evaluation of Methods for Collecting Aerosolized *Bacillus* Spores. *Abstracts of the 34th Annual Conference of the American Association for Aerosol Research* (Minneapolis, Minnesota, U.S.A., October 12-16, 2015), 2IF.1.

Grinshpun, S.A., Yermakov, M., Indugula, R., Reponen, T., Dreizin, E., and Schoenitz, M. (2015) Inactivation of Aerosolized *Bacillus Thuringiensis* Spores by Combustion of Powderized Materials Containing Boron and Iodine. *Abstracts of the 34th Annual Conference of the American Association for Aerosol Research* (Minneapolis, Minnesota, U.S.A., October 12-16, 2015), 3IF.6.

DEPARTMENT OF DEFENSE

DEFENSE THREAT REDUCTION
AGENCY
8725 JOHN J. KINGMAN ROAD
STOP 6201
FORT BELVOIR, VA 22060
ATTN: A. DALTON

DEFENSE TECHNICAL
INFORMATION CENTER
8725 JOHN J. KINGMAN ROAD,
SUITE 0944
FT. BELVOIR, VA 22060-6201
ATTN: DTIC/OCA

DEPARTMENT OF DEFENSE CONTRACTORS

QUANTERION SOLUTIONS, INC.
1680 TEXAS STREET, SE
KIRTLAND AFB, NM 87117-5669
ATTN: DTRIAC